

The Pacific Decadal Oscillation, Revisited

MATTHEW NEWMAN,^{a,b} MICHAEL A. ALEXANDER,^b TOBY R. AULT,^c KIM M. COBB,^d CLARA DESER,^e EMANUELE DI LORENZO,^d NATHAN J. MANTUA,^f ARTHUR J. MILLER,^g SHOSHIRO MINOBE,^h HISASHI NAKAMURA,ⁱ NIKLAS SCHNEIDER,^j DANIEL J. VIMONT,^k ADAM S. PHILLIPS,^e JAMES D. SCOTT,^{a,b} AND CATHERINE A. SMITH^{a,b}

^a CIRES, University of Colorado Boulder, Boulder, Colorado

^b NOAA/Earth Systems Research Laboratory, Boulder, Colorado

^c Department of Earth and Atmospheric Sciences, Cornell University, Ithaca, New York

^d School of Earth and Atmospheric Sciences, Georgia Institute of Technology, Atlanta, Georgia

^e Climate and Global Dynamics, National Center for Atmospheric Research, Boulder, Colorado

^f NOAA/Southwest Fisheries Science Center, Santa Cruz, California

^g Scripps Institution of Oceanography, La Jolla, California

^h Graduate School of Science, Hokkaido University, Sapporo, Japan

ⁱ Research Center for Advanced Science and Technology, University of Tokyo, Tokyo, and Application Laboratory, JAMSTEC, Yokohama, Japan

^j Department of Oceanography and International Pacific Research Center, University of Hawai'i at Mānoa, Honolulu, Hawaii

^k Department of Atmospheric and Oceanic Sciences, and Nelson Institute Center for Climatic Research, University of Wisconsin–Madison, Madison, Wisconsin

(Manuscript received 23 July 2015, in final form 19 February 2016)

ABSTRACT

The Pacific decadal oscillation (PDO), the dominant year-round pattern of monthly North Pacific sea surface temperature (SST) variability, is an important target of ongoing research within the meteorological and climate dynamics communities and is central to the work of many geologists, ecologists, natural resource managers, and social scientists. Research over the last 15 years has led to an emerging consensus: the PDO is not a single phenomenon, but is instead the result of a combination of different physical processes, including both remote tropical forcing and local North Pacific atmosphere–ocean interactions, which operate on different time scales to drive similar PDO-like SST anomaly patterns. How these processes combine to generate the observed PDO evolution, including apparent regime shifts, is shown using simple autoregressive models of increasing spatial complexity. Simulations of recent climate in coupled GCMs are able to capture many aspects of the PDO, but do so based on a balance of processes often more independent of the tropics than is observed. Finally, it is suggested that the assessment of PDO-related regional climate impacts, reconstruction of PDO-related variability into the past with proxy records, and diagnosis of Pacific variability within coupled GCMs should all account for the effects of these different processes, which only partly represent the direct forcing of the atmosphere by North Pacific Ocean SSTs.

1. Introduction

Since its identification in the late 1990s as the dominant year-round pattern of monthly North Pacific sea surface temperature (SST) variability, the Pacific decadal

oscillation (PDO) has been connected both to other parts of the climate system and to impacts on natural resources and marine and terrestrial ecosystems. Subsequent research, however, has found that the PDO is not a single physical mode of climate variability but instead largely represents the combination of three groups of processes: 1) changes in ocean surface heat fluxes and Ekman (wind driven) transport related to the Aleutian low, due to both local unpredictable weather noise and to remote forcing from interannual to decadal tropical variability (largely El Niño) via the “atmospheric bridge”; 2) ocean memory, or processes determining oceanic thermal inertia including

 Denotes Open Access content.

Corresponding author address: Matthew Newman, NOAA/ESRL, 325 Broadway, R/PSD1, Boulder, CO 80305.
E-mail: matt.newman@noaa.gov

“reemergence,” which act to integrate this forcing and thus generate added PDO variability on interannual and decadal time scales; and 3) decadal changes in the Kuroshio–Oyashio system, forced by winds over the North Pacific driving westward-propagating oceanic Rossby waves, manifested as SST anomalies along the subarctic front at about 40°N in the western Pacific Ocean. Thus, the PDO represents the effects of different processes operating on different time scales, and its apparent impacts elsewhere only partly represent direct forcing of the atmosphere by the North Pacific Ocean. What has often been characterized as PDO impacts in the literature may, in fact, reflect correlations with processes that drive simultaneous variations in both the PDO and the impact variables. Consequently, care should be taken when positing the PDO as a forcing of nonoceanic responses without a convincing argument for the physical forcing mechanism.

This paper synthesizes this current view of the PDO and discusses its implications for climate diagnosis, including PDO climate impacts and predictability (both oceanographic and atmospheric); potential decadal-regime-like behavior; PDO simulations in climate models; the interpretation of multicentennial PDO reconstructions; and its relationship to another widely used index, the interdecadal Pacific oscillation (IPO). We conclude with a few suggested best practices for future PDO-based diagnoses and forecasts.

2. What is the PDO?

The PDO was first introduced by Mantua et al. (1997) as the leading empirical orthogonal function (EOF) of North Pacific (20°–70°N) SST monthly averaged anomalies, or SSTAs, defined as departures from the climatological annual cycle after removing the global mean SSTs. Figure 1a shows the PDO pattern, calculated by regressing SST anomalies on the associated principal component (PC) time series, obtained from the HadISST dataset (Rayner et al. 2003), for the years 1901–2014. (Unless otherwise noted, this SST dataset and period are used for all calculations in this paper.) Over this period, the PDO is fairly similar across four SST datasets, all using different methods to fill in missing grids, with relatively minor differences both in time series (Fig. 1b) and pattern. The latter point can be illustrated using the Taylor diagram (Taylor 2001) in Fig. 2, which shows that the root-mean-square (RMS) differences between the HadISST PDO pattern and PDO patterns determined from the other SST datasets are relatively small. The PDO is also reasonably robust to sampling; for example, continually repeating the EOF analysis upon randomly

chosen (with replacement) 50-yr draws from the HadISST dataset yields patterns that are all highly similar to the PDO EOF (as shown by the black dots in Fig. 2). Dataset dependencies are more pronounced early in the observational record, especially prior to about 1920 (Fig. 1b, bottom) or when only a few decades are used to define the climatology and leading EOF (Wen et al. 2014).

Initial research in the 1990s suggested that the PDO might represent a distinct physical “mode” of North Pacific variability. First, even using monthly anomalies, the PDO time series has a slowly varying component, with episodic changes of sign, hence “decadal oscillation.”¹ Second, low *simultaneous* correlation between time series of the PDO and the eastern equatorial Pacific SST anomalies resulted in the PDO and the tropics appearing to be only weakly coupled. Additionally, some early modeling work (Latif and Barnett 1994, 1996) raised the possibility that the PDO might correspond to a physical mode, oscillating on decadal time scales, of coupled atmosphere–ocean interaction within the North Pacific.

As the leading North Pacific EOF, the PDO is, by construction, the single pattern that best encapsulates the variability of monthly SSTAs within the domain where it is defined. However, the PDO is also associated with variability outside the North Pacific, and indeed the observed regression pattern in Fig. 1a shows a strong connection between the North Pacific and the tropics, despite relatively low correlation values within the narrow cold tongue located in the eastern equatorial Pacific between 2°N and 2°S (not shown; see Deser et al. 2004). In particular, positive SSTAs in the eastern tropical Pacific accompany negative SSTAs in the central and western North Pacific and positive SSTAs in the eastern North Pacific (Fig. 1a). Some PDO details depend on the domain used for the EOF calculation: as this domain is expanded southward (Fig. 2, orange symbols), the tropical portion of the pattern becomes relatively more pronounced, even along the equator, with the North Pacific anomaly shifting slightly eastward to become more symmetric with its South Pacific counterpart. The leading SST EOF of the entire Pacific basin resembles a global ENSO-related pattern (e.g., Deser and Blackmon 1995).

While the PDO exists throughout the year, it undergoes some seasonal evolution both in its amplitude

¹Note that in meteorological parlance, “oscillation” was first related to spatial seesaw patterns in the Atlantic and Pacific by Walker and Bliss (1932), but has more recently been occasionally confused with temporal oscillations.

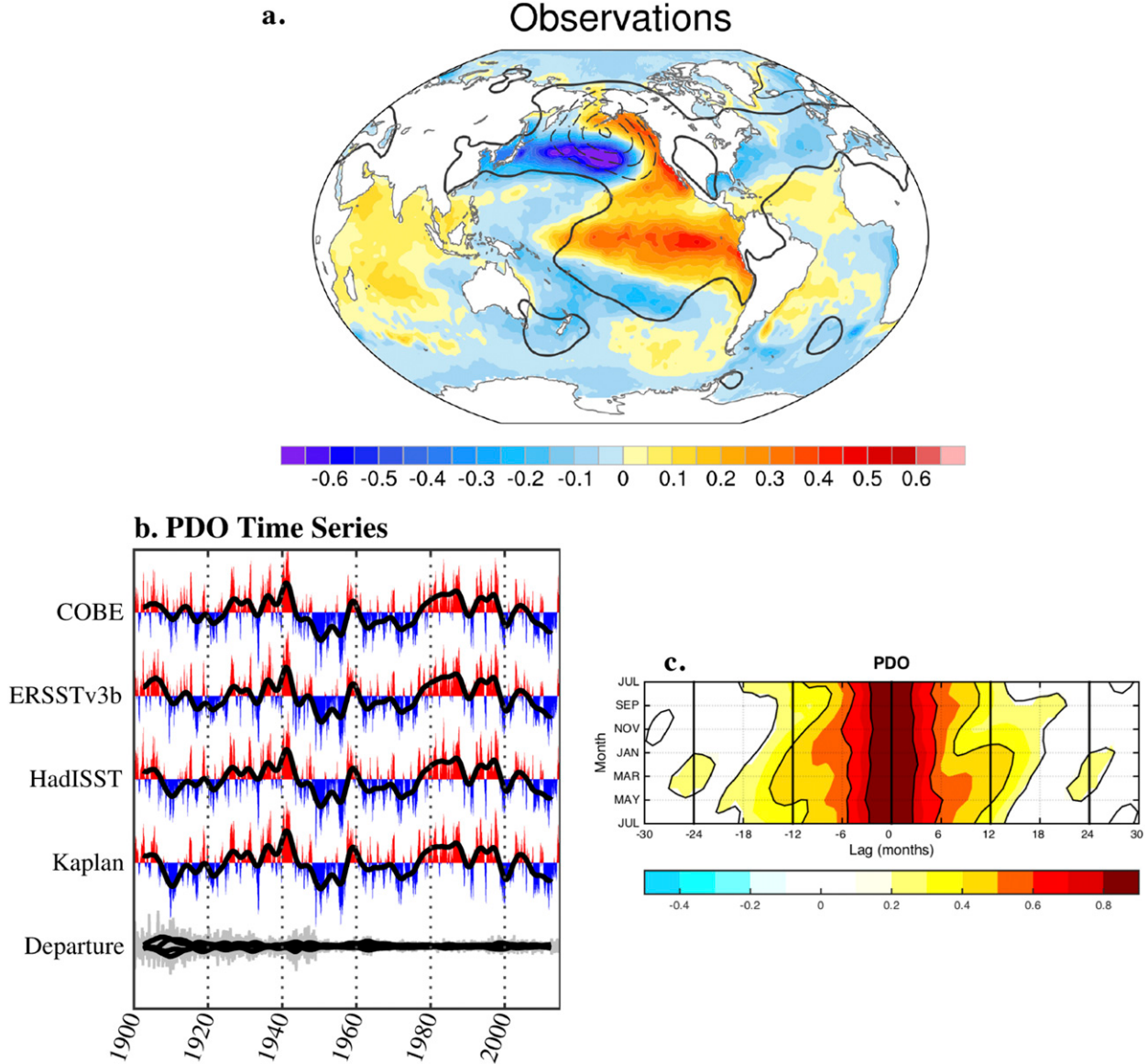


FIG. 1. The PDO over the historical record (1901–2014). (a) Regression of global monthly SST (shading; interval is 0.05°C) and DJF SLP (contours; interval is 1 hPa) anomalies onto the PDO time series from the HadISST dataset. Note that a positive PDO is associated with negative central North Pacific SSTA. (b) PDO index time series determined from the SST datasets, Centennial Observation-Based Estimates (COBE; Ishii et al. 2005), ERSST.v3b (Smith et al. 2008), HadISST (Rayner et al. 2003), and Kaplan (Kaplan et al. 1998). Positive (negative) values are drawn in red (blue). The thick black line in each panel shows the smoothed (6-yr lowpass; Zhang et al. 1997) time series. The last series in (b) shows the departure of each time series from the mean of all four time series. (c) Seasonal cycle of (3-month running mean) PDO index autocorrelation. Contour (shading) interval is 0.2 (0.1). Only values that are 95% significant are shaded. The month ordinate indicates the time of the PDO base month, and the lag indicates how far ahead or behind the PDO is; for example, the value plotted at (5, MAY) represents the correlation between the May value of the PDO and the subsequent October value of the PDO.

and structure. The PDO's amplitude is greatest from November through June, with weak maxima both in midwinter and late spring and a pronounced late summer–early fall minimum (H. Wang et al. 2012). However, repeating the PDO regression separately by month shows the SSTA maximum shifting from the northeastern to northwestern Pacific between the

cold and warm seasons (not shown). In fact, the largest PDO-related SSTAs in the northwestern Pacific occur in early fall despite the overall PDO minimum then. In the observed PDO autocorrelation structure (Fig. 1c), for long lags persistence is increased (decreased) in spring (autumn) (i.e., the tilted ridges or troughs at long leads or lags in Fig. 1c).

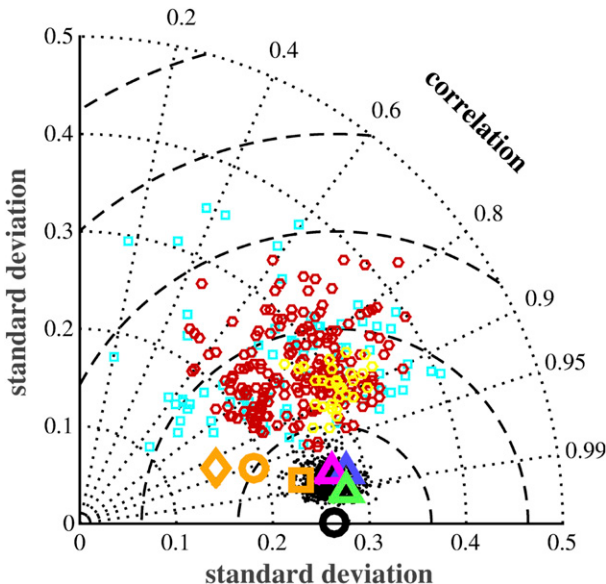


FIG. 2. Taylor diagram (Taylor 2001) comparing the reference PDO (HadISST) pattern (Fig. 1a, black circle) with variations due to sampling, observational dataset, and geographical domain; and to PDOs determined from CGCMs run with historical radiative forcing. In this diagram, the distance of a point from the origin is the pattern standard deviation ($^{\circ}\text{C}$), and the distance from the reference point [at $(0.26, 0)$] is the root-mean-square error (RMSE) between the pattern and the reference pattern, indicated by the dashed semicircles spaced at an interval of 0.1°C . The pattern correlation, decreasing in a counterclockwise azimuthal direction, is mathematically related to these two quantities. The analysis is taken only over the North Pacific PDO domain (20° - 70°N). Black dots show the PDO estimates based on the 50-yr Monte Carlo subsamples; triangles show PDO results determined from the ERSST.v3b (blue), COBE (green), and Kaplan (magenta) observed datasets; orange symbols show the SSTA structure (within the North Pacific PDO region) associated with the leading SSTA EOF, where the southern border of the Pacific domain is instead 0° (square), 20°S (diamond), and 70°S (circle). Also shown are the CMIP3 (cyan squares), CMIP5 (red hexagons), and CESM-LE (yellow hexagons) historical simulation PDOs. EOF spatial patterns were interpolated onto the $2^{\circ} \times 2^{\circ}$ grid used for the reference pattern. As a result of differences in landmasks, metrics for the Taylor diagram were calculated over ocean points that were in common between each model and the HadISST data.

3. Processes driving the PDO

Statistical modes may represent physical modes, but there need not be a one-to-one correspondence between them. A body of research exists showing how different physical processes, including random atmospheric forcing, teleconnections from the tropical Pacific, and ocean Rossby waves/shifts in the basin-wide ocean gyre circulation, contribute to PDO variability on a variety of time scales and regions in the North Pacific Ocean.

a. Fluctuations in the Aleutian low (large-scale stochastic forcing)

Many aspects of climate can be represented by a slow dynamical system integrating fast forcing approximated as random, or stochastic, noise (Hasselmann 1976). In a simple stochastic model of midlatitude SST variability (Frankignoul and Hasselmann 1977), the ocean at a given location is treated as a motionless (well-) mixed layer in which surface heat fluxes both force and damp SSTAs. The forcing F is represented by fluxes associated with weather variations, which relative to oceanic time scales have approximately no memory and the same variance at all time scales (effectively, white noise). The resulting SSTAs are damped by a linear negative air-sea feedback, representing loss (gain) of heat with the atmosphere from anomalously warm (cold) waters. This can be expressed as a first-order autoregressive or AR1 model,

$$\text{SSTA}(n) = r\text{SSTA}(n - 1) + F, \quad (1)$$

where r represents the expected fraction of the SSTA retained between times $n - 1$ and n , determined by the feedback of air-sea heat fluxes and SST and by the thermal inertia of the upper ocean in direct contact with the atmosphere. Then, the SSTAs exhibit a red noise spectrum whose magnitude increases with the inverse square of frequency, flattening out at periods that are long compared to the damping time scale.

The simple view of SST variability as the result of noise integration can be applied basin wide. White noise forcing associated with large-scale weather patterns generates much of the observed SST variability over the entire North Pacific Ocean (Frankignoul and Reynolds 1983), where interannual variability in the surface fluxes and SSTs are closely linked to dominant atmospheric circulation patterns (Cayan 1992; Iwasaka and Wallace 1995). For example, in an atmospheric general circulation model (AGCM) coupled to a mixed layer ocean model with no currents (and hence no ENSO variability or ocean dynamics), the dominant sea level pressure (SLP) pattern is associated with fluctuations in the strength of the Aleutian low pressure system primarily resulting from internal atmospheric dynamics (Pierce 2001; Alexander 2010), including large-scale dominant atmospheric teleconnection patterns such as the Pacific–North American (PNA) pattern. For periods with a stronger Aleutian low, enhanced wind speeds and reduced air temperature and humidity along approximately 35°N cool the underlying ocean via surface sensible and latent heat fluxes, while northward advection of warm moist air heats the ocean near North America (cf. Fig. 1a); the opposite flux anomalies occur when the low is weaker than average.

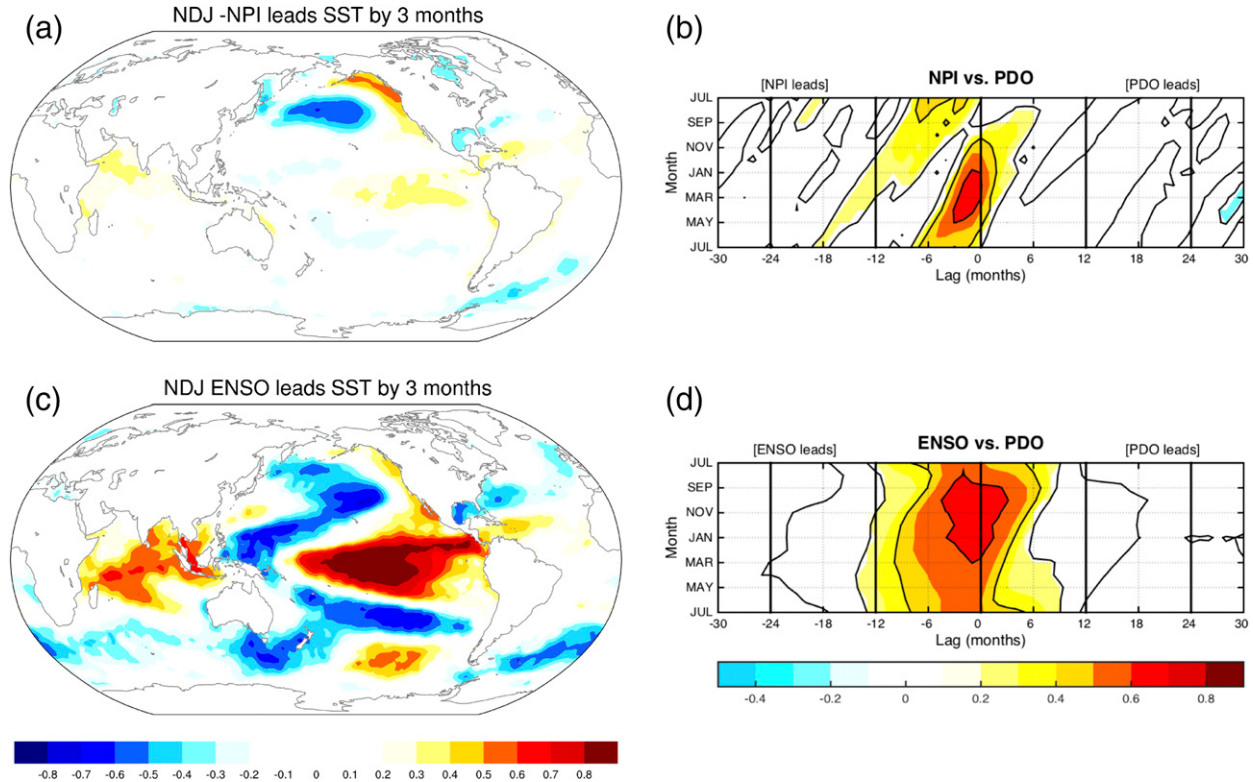


FIG. 3. Illustration of how both local and remote atmospheric forcing can drive PDO variability. (a) One-season lead correlation between November–January (NDJ) NPI and global SSTAs during FMA. (b) Seasonal cycle of cross correlation between the NPI and the PDO index (both filtered with 3-month running mean). PDO leads NPI for positive lags; NPI leads PDO for negative lags. In (a) and (b), the NPI index sign has been flipped so that positive refers to a deepening of the Aleutian low, which also will correspond to positive PDO. (c) One-season lag correlation between the NDJ value of the ENSO index (the leading PC of the tropical Pacific SSTAs) and global SSTAs during FMA. (d) Seasonal cycle of cross correlation between the ENSO and PDO indices (both filtered with 3-month running mean). PDO leads ENSO for positive lags; ENSO leads PDO for negative lags. All panels are determined from 1901–2014 data; shading interval is 0.1. For (b) and (d), only values that are 95% significant are shaded, and the contour line interval is 0.2. The month ordinate indicates the time of the PDO index base month, and the lag indicates how far ahead or behind the second variable is; for example, the value plotted at (5, MAY) represents the correlation between the May value of the PDO and the subsequent October value of the other variable.

This simulated flux-driven SST pattern in the North Pacific closely resembles the observed PDO. Anomalous Ekman transports tend to amplify the flux-driven pattern (Miller et al. 1994a; Alexander and Scott 2008).

These physical processes result in observed correlations in which atmospheric variations generally lead SST variations (e.g., Davis 1976; Deser and Timlin 1997). For example, Fig. 3a shows the PDO-like pattern that results from springtime SST correlation with prior wintertime Aleutian low variability [here measured by the North Pacific index (NPI); Trenberth and Hurrell 1994]. Throughout the cold season, Aleutian low anomalies typically lead the PDO, even over consecutive years (Fig. 3b). Note that the NPI and PDO are also simultaneously correlated, which has been misinterpreted as indicating that the PDO must force an Aleutian low response. As Frankignoul (1999) noted, even without oceanic feedback onto the atmosphere, simultaneous

extratropical atmosphere–SST correlation can occur as a result of rapid weather forcing of the more slowly evolving ocean; so, to diagnose interactions between the North Pacific Ocean and the Aleutian low requires determining both positive and negative PDO–NPI lag correlations.

b. Teleconnections from the tropics

1) THE ATMOSPHERIC BRIDGE

We now generalize the “PDO as integrator” paradigm in (1), allowing for other sources of forcing F beyond noise due to intrinsic midlatitude atmospheric variability. ENSO tropical Pacific SSTAs induce tropical precipitation shifts forcing global atmospheric teleconnections (e.g., Trenberth et al. 1998; Liu and Alexander 2007), altering near-surface air temperature, humidity, wind, and clouds far from the equatorial

Pacific. The resulting variations in the surface heat, momentum, and freshwater fluxes cause changes in SST and ocean currents. Thus, during ENSO events an atmospheric bridge extends from the equatorial Pacific to other ocean basins including the North Pacific (e.g., Alexander 1990, 1992; Lau and Nath 1994, 1996, 2001; Alexander et al. 2002). When El Niño events peak during boreal winter, the Aleutian low deepens and the changes in the surface heat fluxes, wind-driven mixing, and Ekman transport in the upper ocean all act to create a positive PDO SSTA pattern (Alexander et al. 2002; Alexander and Scott 2008; see also Strong and Magnusdottir 2009).

The atmospheric bridge is seen when correlating a wintertime “ENSO index” (here, defined as the time series of the leading tropical SSTA EOF determined within the 18°S–18°N domain) with subsequent global springtime SSTAs (Fig. 3c). This correlation pattern is stable throughout the observational record, with some amplitude changes but relatively little modification in pattern (not shown). In general, ENSO leads the PDO throughout the year (Fig. 3d), but the bridge acts differently in summer and fall compared to winter, modifying SSTAs in the western Pacific primarily through changes in cloudiness (Alexander et al. 2004).

2) OCEANIC COASTALLY TRAPPED WAVES

The equatorial thermocline variability associated with ENSO excites Kelvin and other coastally trapped ocean waves that propagate poleward along the eastern Pacific boundary in both hemispheres, generating substantial sea level and SST anomalies (Enfield and Allen 1980; Chelton and Davis 1982; Clarke and Van Gorder 1994). However, these waves impact the ocean only within about 50 km of shore poleward of 15°N (Gill 1982).

3) TROPICAL DECADAL VARIABILITY

Tropical Pacific decadal variations will also be communicated to the North Pacific via the atmospheric bridge, driving about 1/4–1/2 of the PDO-related variability based on GCM model experiments (Alexander et al. 2002; Alexander 2010). Zhang et al. (1997) employed several techniques to separate observed interannual and interdecadal (>6 yr) ENSO variability. The SSTA pattern based on their low-pass-filtered data is similar to the unfiltered ENSO pattern, except meridionally broader in the eastern equatorial Pacific and with higher amplitudes both in the central equatorial Pacific and in the extratropics; its North Pacific component resembles the PDO. Other statistical methods have found similar structures and have indicated that some PDO decadal variability is associated with low-frequency anomalies in the tropical Pacific (e.g., Nakamura et al. 1997; Power et al. 1999;

Mestas-Nuñez and Enfield 1999; Barlow et al. 2001; Seager et al. 2004; Deser et al. 2004; Vimont 2005; Alexander et al. 2008; Chen and Wallace 2015).

How much tropical Pacific decadal variability is due to coupled processes operating on fundamentally decadal time scales, including possible linkages to the North Pacific [see section 3c(4)], and how much is the residual of weather noise-driven ENSO dynamics (e.g., Newman et al. 2011; Wittenberg et al. 2014) remains to be determined. Because the decadal ENSO pattern is similar to the most persistent portions of the seasonally evolving ENSO pattern, it may be partly the residual of a non-uniformly evolving interannual phenomenon (Vimont 2005) and/or the asymmetry between warm and cold phases of ENSO (Rodgers et al. 2004).

c. Midlatitude ocean dynamics and coupled variability

1) REEMERGENCE

We might expect that, because of the thermal capacity of seawater and typical mixed layer depths, the memory time scale of the upper ocean is on the order of months. However, because of seasonal variations in the oceanic mixed layer depth, the decorrelation time scale of midlatitude SSTAs in successive cold seasons is generally greater than a year. Figures 4a–c illustrate this process, showing the correlation of February–April (FMA) PDO values with ECMWF Ocean Reanalysis System, version 4 (ORAS4; Balmaseda et al. 2013), ocean temperatures at depth and increasing lag for three regions of the North Pacific. Similar results are obtained using the SODA dataset (Carton and Giese 2008; not shown) and in modeling studies (e.g., Alexander et al. 2002; H. Wang et al. 2012). Persistent temperature anomalies forming at the surface mix downward throughout the deep winter mixed layer. Then, when the mixed layer abruptly shallows in spring, thermal anomalies at depth can remain under the summer seasonal thermocline, insulated from surface fluxes that damp anomalies in the thin mixed layer above. When the mixed layer deepens again during the following fall, the deeper anomalies are mixed back toward the sea surface. This process, first noted by Namias and Born (1970, 1974) and termed the “reemergence mechanism” by Alexander and Deser (1995), occurs over large portions of the North Atlantic and North Pacific Oceans (Alexander et al. 1999, 2001; Bhatt et al. 1998; Timlin et al. 2002; Hanawa and Sugimoto 2004). The PDO SSTA pattern, generated by internal atmospheric dynamics and/or the atmospheric bridge, recurs in consecutive winters via the reemergence mechanism (Alexander et al. 1999, 2001, 2002), while the summertime PDO signal (at the surface, at least) does not

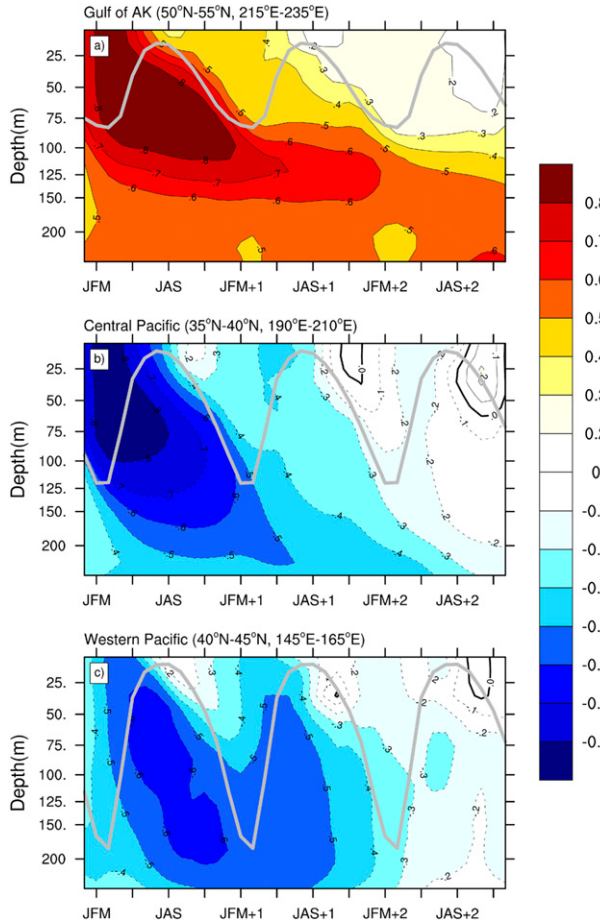


FIG. 4. Illustration of the reemergence of oceanic thermal anomalies. Correlation of the February–April (FMA) value of the PDO index (as in Fig. 1b, but determined from 3-month running means) with ECMWF ORAS4 ocean temperatures (Balmaseda et al. 2013) for the subsequent 3 yr, area averaged in (a) the Gulf of Alaska, (b) the central Pacific, and (c) the western Pacific, for the years 1958–2014, with the 57-yr linear trend removed from each area average. The gray line shows the climatological mean mixed layer depth as a function of time of year at each location, so it repeats over the 3-yr period.

tend to recur (Nakamura and Yamagata 1999) and is instead largely forced by contemporaneous air–sea fluxes. The effects of reemergence can extend into a second year, as evidenced in Fig. 4 by the cold season maxima during both years 1 and 2.

Thus, the reemergence mechanism determines the effective thermal inertia and the value of r in (1) as corresponding to deep winter mixed layers (Deser et al. 2003), enhancing PDO variability on interannual to decadal time scales (Newman et al. 2003; Schneider and Cornuelle 2005). The impact of reemergence is evident in the observed PDO lag autocorrelation structure (Fig. 1c). For example, while the year-to-year PDO autocorrelation is over 0.45 in late winter and spring, it drops below 0.3 in late summer and autumn. Also, the PDO is significantly

correlated over three consecutive springs but is nearly uncorrelated over three consecutive autumns.

2) OCEAN GYRE DYNAMICS

Much of the large-scale dynamics within the North Pacific Ocean involves two basin-wide circulations of water, a counterclockwise subpolar gyre and a clockwise subtropical gyre, separated by a sharp meridional SST gradient called the subarctic frontal zone (SAFZ). In the western Pacific, large SST variations associated with the PDO occur within the SAFZ, specifically in the Kurashio Extension (KE) and Oyashio frontal zones and the mixed water region in between (Nakamura et al. 1997; Nakamura and Kazmin 2003; Nonaka et al. 2006; see, e.g., Fig. 5 in Frankignoul et al. 2011). While in most of the North Pacific, SST variability is driven primarily by atmospheric forcing (Smirnov et al. 2014), in this region persistent warm (cool) SSTAs in winter tend to enhance (reduce) heat and moisture fluxes into the atmosphere (Tanimoto et al. 2003; Taguchi et al. 2012), a consequence of the dynamic adjustment of upper-ocean gyre circulations that contributes to F in (1). The adjustment occurs primarily through westward-propagating Rossby waves excited by anomalous wind stress curl (Miller et al. 1998; Deser et al. 1999; Seager et al. 2001; Schneider et al. 2002; Qiu and Chen 2005; Taguchi et al. 2007). These waves, whose sea surface height variations can be measured by satellite (Fig. 5b), take approximately 3–10 yr to cross the basin guided by the KE jet (Sasaki and Schneider 2011; Sasaki et al. 2013), producing primarily decadal variability in F with a red spectra without preferred spectral peaks (Frankignoul et al. 1997). Specifically, SSTAs result (Fig. 5a) from shifts in latitude and intensity of the fronts (Qiu 2003; Nakamura and Kazmin 2003; Taguchi et al. 2007), and modulations of the stability of the KE jet, the recirculation gyre (Qiu 2000, 2002; Qiu and Chen 2005, 2010; Kelly et al. 2010; Kwon et al. 2010a), and thereby oceanic eddy-driven heat transports (Sugimoto and Hanawa 2011). The latitude of the shallow Oyashio front, by contrast, may be more sensitive to local wind forcing (Nonaka et al. 2006, 2008). Decadal SSTAs in the KE and Oyashio regions have undergone long-term amplitude modulations, suggesting that this contribution from extratropical air–sea interaction to the PDO may vary on multidecadal scales (Miyasaka et al. 2014).

An atmospheric response to PDO SST variations could enhance PDO decadal variance, or lead to a preferred time scale, if the response projects onto F in (1) as a positive or delayed negative, respectively, feedback on the PDO. A basic thermodynamic response exists: the temperature difference between the atmospheric boundary layer and oceanic mixed layer decreases because of air–sea heat exchange, slowing subsequent heat

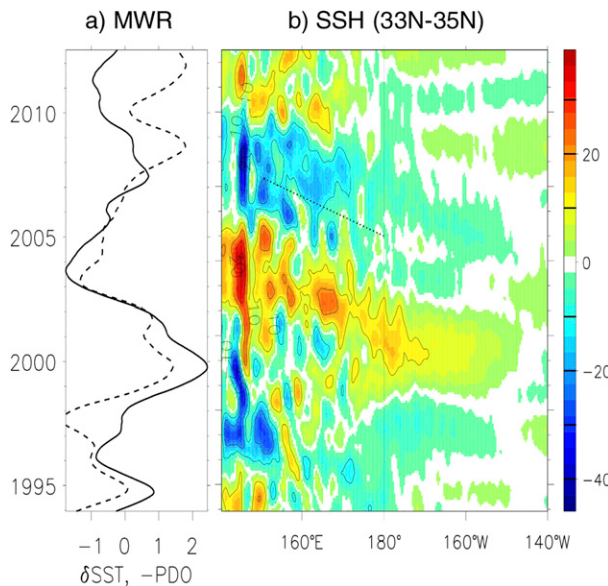


FIG. 5. Illustration of the slow ocean (Rossby wave) dynamics process driving PDO variability. (a) Time series of the SST in the mixed-water region (MWR, solid) and the PDO index (with sign inverted, dashed). The temperature index is based on the optimal interpolation, blended, $1/4^{\circ}$ SST analysis of Reynolds et al. (2007). The MWR extends from the coast of Japan to 150°E , and between 36° and 42°N . Both the MWR and PDO indices have been normalized by their respective standard deviations. The correlation between MWR and PDO indices is -0.49 . (b) Satellite-observed sea surface height anomalies (cm), averaged between 33° and 35°N . The dotted line marks a westward phase speed of 3.7 cm s^{-1} (Qiu and Chen 2010). Sea surface temperature and sea surface height anomalies have been detrended and smoothed with a 2-yr running mean, with weights varying linearly as a function of lag.

exchanges that depend upon this difference, producing “reduced thermal damping” (Barsugli and Battisti 1998) and a related increase in temperature variability (Bladé 1997). Stochastic wind forcing whose spatial scale corresponds to certain ocean advective scales might also resonantly enhance decadal SST variability without other feedbacks (Saravanan and McWilliams 1998).

The coupled ocean–atmosphere dynamical response to PDO SSTAs has been less clear. Latif and Barnett (1994, 1996) suggested that western Pacific SST anomalies resulting from Aleutian low-forced Rossby wave adjustment of the subtropical gyre (described above) drive an atmospheric response that, via the wind stress curl, reverses the sign of the subtropical gyre anomaly and the corresponding central North Pacific SST anomaly. This negative feedback in the western Pacific initiates the opposite phase of a 20-yr PDO oscillation. However, the necessary western Pacific atmospheric response appears to be of the wrong sign to generate sustained oscillations (Schneider et al. 2002). In particular, when the Aleutian low strengthens, it also shifts southward; as a result,

the gyre circulation shifts equatorward, and the SST anomalies subsequently cool rather than warm in the KE region (Deser et al. 1999; Miller and Schneider 2000; Seager et al. 2001). In addition, surface heat fluxes damp SST anomalies in the KE region both in observations and ocean model hindcasts (Seager et al. 2001; Schneider et al. 2002; Tanimoto et al. 2003). Note also that the length of the Latif and Barnett model run was relatively short; their results were not reproduced in a longer run of the model (Schneider et al. 2002), whereas large model ensembles are now used to discern SSTA-forced signals from undersampled atmospheric noise (e.g., Sarshemukh et al. 2000; Deser et al. 2004).

Still, recent observational studies (Frankignoul et al. 2011; Taguchi et al. 2012), coupled model experiments (Wu et al. 2003; Kwon and Deser 2007; Taguchi et al. 2012), and observationally derived heuristic models (Qiu et al. 2007) suggest that the atmospheric response to SSTAs in the KE and Oyashio frontal zones could induce a modest atmospheric response in the anomalous Aleutian low, which may be able to enhance the variability at decadal periods. Those SST frontal zones may act to anchor the Pacific storm track (Nakamura et al. 2004), and its feedback forcing from synoptic-scale eddies migrating along the storm track seems important in maintaining a stationary atmospheric response (Taguchi et al. 2012; Okajima et al. 2014). However, AGCM studies continue to disagree on even the sign of the atmospheric response to frontal zone SSTAs, with sensitivity to many factors including the simulated direct response to the low-level heating, downstream eddy feedbacks of the modulated storm track, and dependencies upon seasonality and base state (Okajima et al. 2014; see also the review by Kushnir et al. 2002). Also, Frankignoul et al. (2011) and Taguchi et al. (2012) observed an anomalous surface Aleutian low in response to KE–Oyashio front SSTAs that, however, was accompanied by different upper-level anomalies. Some recent observational analyses and model experiments at finer resolutions (typically $\sim 25 \text{ km}$) suggest that a robust atmospheric response to KE–Oyashio front SSTAs may involve significant changes in poleward heat and moisture transports by individual storms (O'Reilly and Czaja 2015) that are not well captured by currently typical climate model atmospheric resolution ($\sim 1^{\circ}$; Smirnov et al. 2015), so the impact of ocean–atmosphere coupling onto the PDO remains poorly understood.

3) SUMMERTIME AIR–SEA FEEDBACKS

During summer, because of both a shallower seasonal thermocline and weaker atmospheric variability, the PDO tends to be less persistent and less confined to the oceanic frontal zones (Nakamura and Kazmin 2003), although the spatial structure of the PDO is not

fundamentally changed (Chen and Wallace 2015). Instead, SST variability may be linked to anomalous low-level cloudiness. Over the northeast (NE) Pacific, for example, where summertime midtropospheric subsidence is maintained by the climatological subtropical high (Miyasaka and Nakamura 2005), most of the clouds develop under the capped inversion layer (Klein et al. 1995; Norris 1998; Wood 2012). Decadal enhancement of lower-tropospheric static stability, due both to cooler SSTAs and stronger subsidence associated with the intensified subtropical high, acts to increase the low-level cloud amount, optical depth, and planetary albedo, and vice versa (cf. Clement et al. 2009). The resulting anomalous cloud radiative forcing could enhance the underlying SSTA as positive feedback. Over the northwest (NW) Pacific, low-level cloudiness is climatologically high in summer, but is less variable than over the NE Pacific (Norris et al. 1998), which is particularly the case over the subpolar oceanic gyre. Still, decadal variability in low-level cloudiness tends to maximize around 35°N to the south of the North Pacific (NP) SAFZ. Schwartz et al. (2014) show that the summertime coastal low clouds all along the West Coast vary in concert with PDO-related SST variations.

4) NORTH PACIFIC IMPACTS ON TROPICAL VARIABILITY

While the atmospheric bridge primarily extends from the tropics to the extratropics, North Pacific SSTA variability may also influence the tropical Pacific. In the “seasonal footprinting mechanism” (Vimont et al. 2001, 2003), wintertime weather noise alters surface heat fluxes to create SST anomalies that in the subtropics persist through the summer. These SST anomalies, which are largely orthogonal to the PDO since they instead reflect the second EOF of North Pacific SSTAs (Bond et al. 2003), associated with the North Pacific Gyre Oscillation (NPGO; Di Lorenzo et al. 2008), drive near-equatorial zonal wind stress anomalies impacting ENSO variability (Vimont et al. 2003, 2009; Alexander et al. 2008, 2010; Di Lorenzo et al. 2010; S.-Y. Wang et al. 2012). On longer time scales, in some models the atmospheric response to slowly varying KE SST anomalies extends deep into the tropics to affect decadal ENSO variability (Barnett et al. 1999; Kwon et al. 2010b).

A coupled extratropical–tropical mechanism for decadal variability proposed by Gu and Philander (1997) involves subduction of North Pacific mixed layer temperature anomalies from the surface layer into the thermocline and their subsequent southward advection by the subtropical cell (STC) to upwell at the equator. However, observational analyses showed that subducted central North Pacific anomalies decay prior to

reaching the tropics (Deser et al. 1996; Schneider et al. 1999; Capotondi et al. 2003; Sasaki et al. 2010; Y. Li et al. 2012). Alternatively, variations in subtropical winds (which may also be noise driven) alter the strength of the STC overturning circulation, changing its southward advection of relatively cold extratropical water that, upwelling at the equator, drives tropical air–sea feedbacks and hence decadal variability. This mechanism, evident in some models (Kleeman et al. 1999), although possibly confined to within about 20° of the equator (Capotondi et al. 2005), is supported by observational analyses (McPhaden and Zhang 2002; Zhang and McPhaden 2006). Note that even if this mechanism does not extend into the North Pacific it still impacts the PDO by modifying its tropical forcing.

4. The PDO as the sum of multiple processes

In this section we employ two approaches, empirical and numerical modeling studies, to explore how PDO processes combine to produce PDO variability and dynamics and, potentially, PDO regime shifts.

a. Empirical autoregressive models

Several recent studies extended the simple AR1 model in (1) to incorporate additional PDO dynamical processes discussed above. Using annually averaged (July–June) observed SSTAs, Newman et al. (2003) found that (1) could be improved by including ENSO forcing within F , extending the AR1 model to

$$\text{PDO}(n) = r\text{PDO}(n-1) + a\text{ENSO}(n) + \text{noise}. \quad (2)$$

Note that r , which corresponded to a time scale of about 2 yr, included reemergence, amplifying the low-frequency ENSO component of PDO variability to produce a “reddened ENSO.” Schneider and Cornuelle (2005) included both shifts in the North Pacific Ocean gyres and explicit representation of anomalous Aleutian low forcing in F to show that on interannual time scales, random Aleutian low fluctuations and ENSO teleconnections were about equally important in determining PDO variability with negligible contributions from ocean currents, while on decadal time scales, stochastic forcing, ENSO, and changes in the gyre circulations each contributed approximately one-third of the PDO variance. The primary implication of these analyses is that, unlike ENSO, the PDO is likely not a single phenomenon but rather the sum of several different basin-scale processes (e.g., Schneider and Cornuelle 2005; Newman 2007, 2013; Alexander et al. 2008).

As (1) is extended into (2) by including observed, nonstochastic forcing in F , it is no longer strictly speaking an AR1 model, nor is it a closed model. Also, while the patterns corresponding to these processes are not identical and their characteristic time scales are quite different, they all project strongly onto the PDO pattern. However, many common multivariate analysis techniques cannot distinguish between spatially similar, or nonorthogonal, patterns with differing patterns of evolution.

These problems can be addressed by extending the AR1 model to many variables:

$$\mathbf{x}(n) = \mathbf{G}\mathbf{x}(n-1) + \boldsymbol{\eta}_s, \quad (3)$$

where \mathbf{x} is now a multivariate state vector and $\boldsymbol{\eta}_s$ represents noise. In the following, \mathbf{x} represents maps of observed SSTAs covering the tropical (18°S – 18°N) and North Pacific (20° – 70°N) Oceans. The resulting multivariate AR1 model [linear inverse model (LIM); Penland and Sardeshmukh 1995; Newman 2007; Alexander et al. 2008] yields patterns representing different dynamical processes with different evolutions, which are independent but not orthogonal; that is, they have potentially similar spatial structures. In analogy with (1), each pattern (each eigenmode of \mathbf{G}) is associated with a time series that has its own value of r (the real part of its eigenvalue), but not all the patterns are static (some also propagate with characteristic frequency given a nonzero imaginary eigenvalue). Here, we extend the Newman (2007) LIM to finer spatial ($2^{\circ} \times 2^{\circ}$) and temporal (3-month running mean) resolution (details of the approach, including strengths and weaknesses, can be found there and the many papers cited therein). Similar to that study and related LIM analyses (Compo and Sardeshmukh 2010; Newman 2013), the leading eigenmode's pattern (not shown) is the departure of the local SST trend from the global mean SST trend and makes almost no contribution to the PDO. Results below are also little changed using a linearly detrended dataset (Newman 2013).

Ordered by decreasing r , the three eigenmodes in Fig. 6 represent dynamical processes with maxima in the northern, central tropical–northern subtropical, and eastern tropical Pacific, respectively; similar patterns from various analyses have been reported elsewhere (e.g., Barlow et al. 2001; Chiang and Vimont 2004; Guan and Nigam 2008; Compo and Sardeshmukh 2010). The first eigenmode represents largely North Pacific dynamics. The latter two represent interannual-to-decadal tropical dynamics driving North Pacific variability (Newman 2007), consistent with Schneider and Cornuelle (2005); their tropical portions form a simple basis for ENSO evolution including its “flavors”

or diversity (e.g., Penland and Sardeshmukh 1995; Trenberth and Stepaniak 2001; Takahashi et al. 2011; Capotondi et al. 2015). Each eigenmode's projection on the PDO EOF yields time series (also in Fig. 6) that when summed result in a “reconstructed” PDO (Fig. 6g) that is quite similar to the full PDO (Fig. 6h), with 0.7 correlation that increases to over 0.8 when both are smoothed with the 6-yr low-pass filter used in Fig. 1b. The residual between the two time series, representing the contributions of other eigenmodes (not shown), is likely primarily noise since its decorrelation time scale is approximately 5 months.

The PDO appears to undergo rapid transitions between extended periods of opposite phase every few decades or so (e.g., Ebbesmeyer et al. 1991; Graham 1994; Mantua et al. 1997; Minobe 1997; Fleming 2009; Minobe 1999), as denoted by the green lines in Fig. 6h. Such “regime shifts” (if significant; see Rudnick and Davis 2003) might represent sudden nonlinear changes between relatively stable climate states. However, similar behavior is also well known to exist in aggregations of AR1 processes (Granger 1980; Beran 1994), that is, in (3). So, to the extent that the PDO represents an aggregation of several basin-scale dynamical processes with differing, but substantial, projections onto the PDO pattern, each PDO regime could result from different combinations of processes (see also Deser et al. 2004), with apparent regime shifts due to randomly forced variations in the superposition of these processes (Newman 2007), as captured by the reconstructed PDO in Fig. 6g. In other words, PDO climate regime shifts could be partly an artifact of measuring the multivariate North Pacific Ocean climate system with a single index.

As a corollary, a PDO regime shift need not correspond to pronounced changes throughout the North Pacific. This point is illustrated by comparing multidecadal SST change across 1976/77 relative to change across 1969/70. The latter time is not typically identified with a Pacific regime shift (although see Baines and Folland 2007), but it is when the time series of the most slowly varying PDO component ended a long period of negative values (Fig. 6a). For the 1976/77 regime shift between 20-yr epochs (Fig. 7b), the well-documented warming in the tropical Indo-Pacific and along the west coast of North America is evident, along with central northeastern Pacific cooling (e.g., Graham 1994; Miller et al. 1994b; Meehl et al. 2009). However, North Pacific multidecadal cooling across 1969/70 (Fig. 7a) was stronger and extended farther westward; note also a corresponding Atlantic signal. The two figures together show that these multidecadal shifts in tropical and North Pacific SSTs were not coincident but rather occurred over several years, and

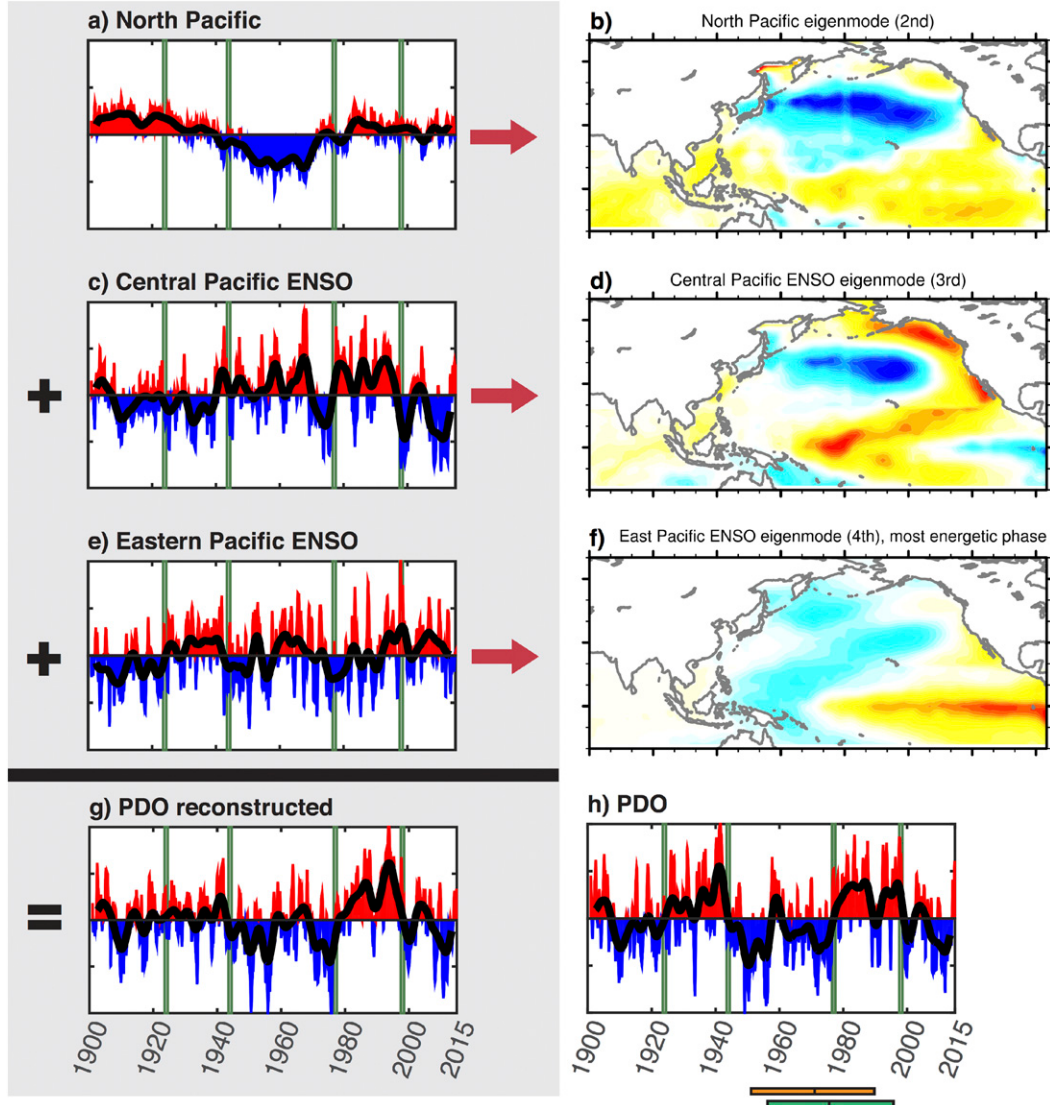


FIG. 6. Reconstructing the PDO as the sum of three different dynamical processes. Time series for the contributions to the PDO from the (a) second (North Pacific), (c) third (central Pacific ENSO), and (e) fourth [eastern Pacific ENSO; showing the most energetic phase of this complex eigenmode (essentially, cosine phase), with the least energetic phase (sine phase) not shown] eigenmodes and (b),(d),(f) the corresponding maps of the LIM described in the text. Note that unlike EOFs, these eigenmodes are nonorthogonal. Contour intervals are the same in all three eigenmode maps; all eigenmodes are normalized to have unit amplitude. For all time series, positive (negative) values are drawn in red (blue). The LIM is determined in a reduced EOF space (with 25 degrees of freedom) that retains about 85% of the SST variance in the tropics and North Pacific domains. (g) PDO reconstruction is the sum of the time series shown in (a),(c),(e). (h) PDO index time series (as in Fig. 1c, but with a 3-month running mean smoothing applied). In the time series panels, thick black lines represent the application of the same 6-yr low-pass smoother as in Fig. 1b, and vertical green lines indicate times of PDO regime shifts.

may not have corresponded to a coherent basin-wide Pacific climate regime shift.

b. PDO representation by coupled climate models

Perhaps our most comprehensive tool for understanding how processes interact to produce the PDO is the coupled general circulation model (CGCM). Here,

we assess a CGCM reproduction of the PDO and PDO processes.

Figure 8 exemplifies the range of PDO patterns (defined according to Mantua et al. 1997) across the historical model runs from phase 5 of the Coupled Model Intercomparison Project (CMIP5), in comparison with the observed pattern (Fig. 1a). All CMIP5

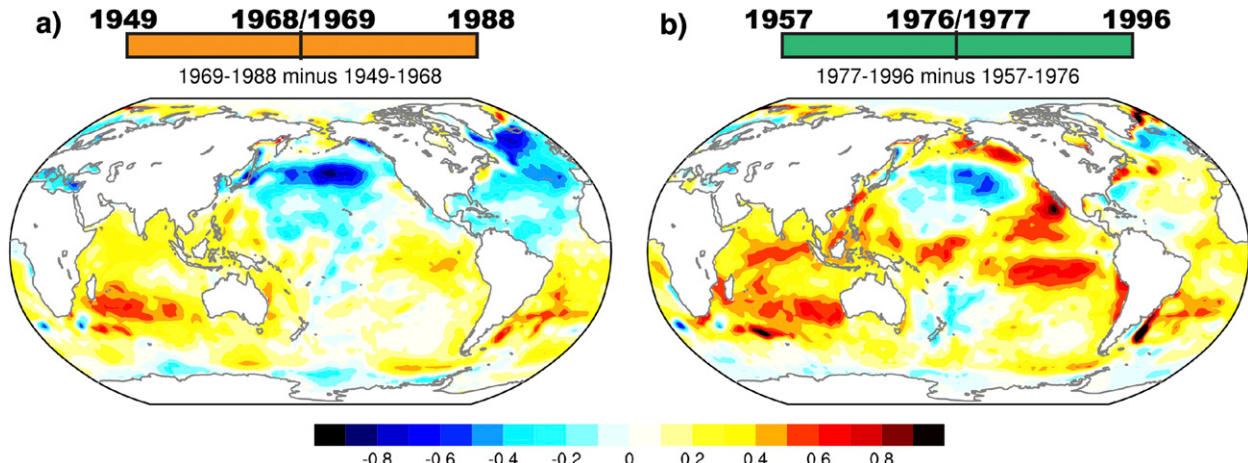


FIG. 7. Epoch difference maps, showing SST differences between two adjacent 20-yr means centered on (a) 1968/69 and (b) 1976/77. Contour interval is 0.1°C . The adjacent 20-yr periods used for each epoch calculation are indicated by the corresponding color bars in Fig. 6h.

PDO patterns are available online (<http://www2.cesm.ucar.edu/working-groups/cvewg/cvdp>) (Phillips et al. 2014). Some models can depict the observed spatial pattern (model A) while others lack the tropical connection (model B). Also shown are two PDO patterns, chosen to be closest (A) and farthest (B) from the observations, generated from two ensemble members taken from the same CGCM, the Community Earth System Model-Large Ensemble (CESM-LE; Kay et al. 2015). Here, the differences are entirely due to internally generated variability, since all other aspects of the experiment (including the model and external forcing) are fixed. We next use the Taylor diagram in Fig. 2 to quantify the degree of resemblance of the PDO pattern in each CMIP3, CMIP5, and CESM-LE model simulation with the observations (HadISST). Recall that the distance of each symbol from the reference (HadISST PDO) represents the RMS difference of each model PDO pattern. The North Pacific SSTA pattern of each model ensemble member is broadly similar to the observations, and is accompanied by a realistic SLP anomaly that is consistent with the atmosphere forcing the ocean and not vice versa (see also Sheffield et al. 2013; Yim et al. 2014), but Fig. 2 shows that the simulations are generally outside the range of the observational dataset and sampling uncertainty. Comparing the CMIP5 and CESM-LE values in Fig. 2 suggests that PDO simulation uncertainty may be due more to differences between models than to differences between realizations. Some modest improvement of the PDO simulation from CMIP3 to CMIP5 is apparent (see also Polade et al. 2013), primarily through the reduction of outliers.

As a result of the chaotic nature of the climate system, even very small differences in initial conditions cause

simulations to diverge from one another and from nature. Hence, in the absence of an externally forced signal, we expect CGCMs to represent PDO variability statistics but not the observed PDO time series. Figure 8c shows this expected range in CMIP5 historical PDO time series (smoothed with the 6-yr low-pass filter); in particular, none reproduce the observed twentieth-century sequence of PDO regimes. Additionally, the ensemble mean of all the time series is near zero. This is also the case for the CESM-LE ensemble mean, although the CMIP3 ensemble mean has a weak trend. Given that these model runs are forced with the post-1850 history of radiative forcing, Fig. 8c suggests that the externally forced PDO signal has been negligible, consistent with the empirical analysis in section 4a, and that the PDO represents natural internal variability.

We show the lag autocorrelation of the PDO (Fig. 9a), as well as the lagged correlations between the PDO and the December–February (DJF) Niño-3.4 index (Fig. 9b) or DJF PNA index (Fig. 9c), for each model ensemble member over its respective period, compared to observations from 1901 to 2009. Most, but not all, simulated PDO time series are too persistent. In all the models during the winter, the PDO is too weakly correlated with both the PNA and Niño-3.4, yet many of the models then overestimate the lagged correlation between these same indices and the PDO the following spring and summer, consistent with too strong PDO persistence or with errors in the North Pacific seasonal cycle.

Previous analysis showed that almost all CMIP3 models underestimated the ENSO–PDO relationship compared to the observations (Newman 2007; Oshima and Tanimoto 2009; Furtado et al. 2011; Lienert et al. 2011; Deser et al. 2012; Park et al. 2013). To investigate how the representation of tropical–extratropical interaction impacts the

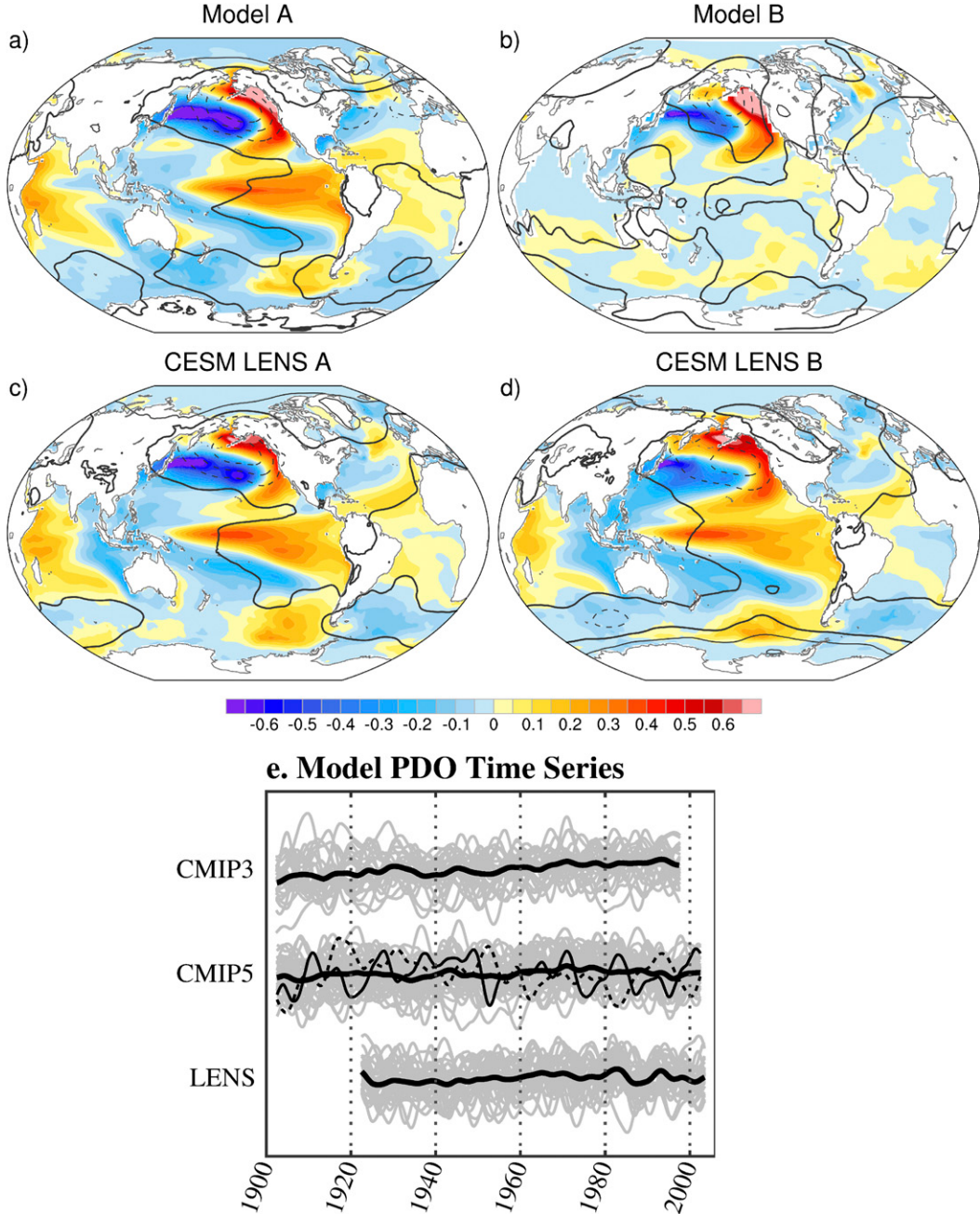


FIG. 8. The PDO over the historical record as simulated by coupled CGCMs. (a),(b) As in Fig. 1a, but showing two selected members of the historical CMIP5 ensemble that are (a) closest and (b) farthest from the reference pattern in Fig. 2. (c),(d) As in (a),(b), but showing two selected members of the CESM-LE that are (c) closest and (d) farthest from the reference pattern in Fig. 2. (e) PDO time series from all ensemble members; all time series are smoothed with the Zhang et al. (1997) filter (used in Fig. 1c). Thin gray lines represent each ensemble member, the thin black solid (dashed) line in the CMIP5 panel represents model A (B), and the thick black line is the ensemble mean for each set of models.

PDO in the CMIP5 historical runs, we fit each PDO time series with the extended AR1 model:

$$\begin{aligned} \text{PDO}(n) = & r\text{PDO}(n-1) + a\text{ENSO1}(n) \\ & + b\text{ENSO2}(n) + \varepsilon(n), \end{aligned} \quad (4)$$

where PDO is the PDO time series, ENSO1 and ENSO2 are the time coefficients of the leading two EOFs of tropical Pacific (20°S – 20°N) SSTAs, ε is white noise, and n is the time step. This model, estimated for detrended and normalized annual mean time series averaged from

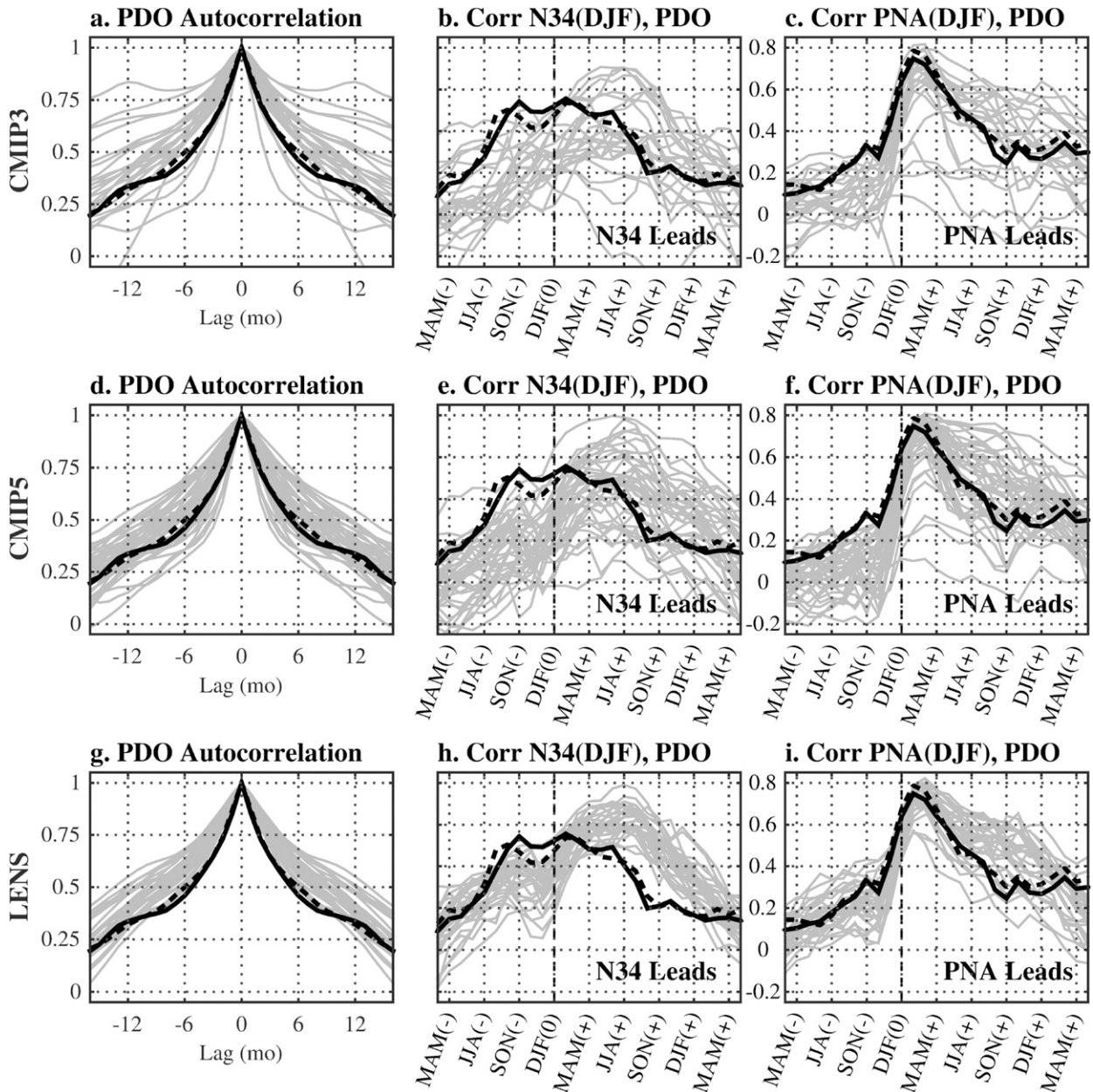


FIG. 9. Temporal relationships relevant to the PDO for the (top) CMIP3, (middle) CMIP5, and (bottom) CESM-LE (LENS) ensembles. Shown are (a),(d),(g) the autocorrelation of the monthly PDO index; (b),(e),(h) the lagged seasonal correlation between the seasonal PDO index and the DJF averaged Niño-3.4 index; and (c),(f),(i) the lagged seasonal correlation between the seasonal PDO index and the DJF-averaged PNA index. In all panels the thin gray lines indicate model correlations, the thick solid black line indicates correlations for indices from the HadISST data, and the thick dashed line indicates correlations with indices from the ERSST.v3b data. In (c),(f),(i) the observed DJF PNA time series is obtained from the twentieth-century reanalysis. Observed correlations are taken over the time period 1901–2009, CMIP3 over 1900–99, CMIP5 over 1901–2004, and LENS over 1920–2005. For seasonal correlations, positive lags indicate that the Niño-3.4 or PNA index leads the seasonal PDO index, and the label along the abscissa indicates the season for which the PDO is defined.

July to June, follows the approach introduced in (2) but includes potential diversity in ENSO anomalies (Capotondi et al. 2015). ENSO1 and ENSO2 are determined separately for each model and dataset and then annually averaged.

The extended AR1 models constructed from the observations and the CMIP5 runs have several notable differences. First, tropical forcing of the PDO is dominated by ENSO1 in the observations, but not for most CMIP5 runs (Fig. 10b). Also, how well each extended AR1 model

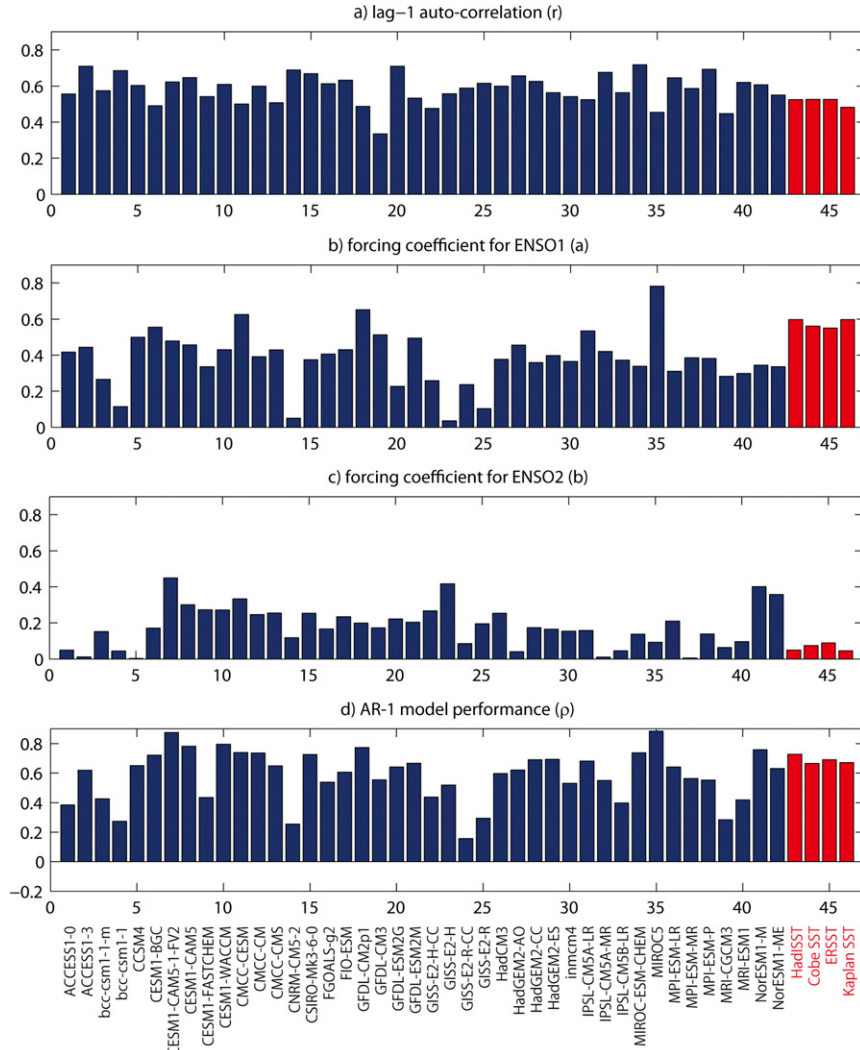


FIG. 10. Parameters for an AR1 model of the PDO time series [(4)] for CMIP5 models (blue bars) and observations (red bars). The AR1 model is determined from the PDO index and two leading tropical PCs, ENSO1 and ENSO2, calculated as discussed in the text but for the period 1900–2000, and then averaged from July to June. (a) Unforced lag-1 autocorrelation, that is, r in (4). (b) Forcing coefficient for ENSO1, that is, a in (4). (c) Forcing coefficient for ENSO2, that is, b in (4). (d) Correlation ρ between each model's PDO index time series and the corresponding estimated PDO time series determined from the AR1 model.

represents each PDO time series is related to ENSO1 forcing strength: in Fig. 10, AR1 model performance ρ , the correlation of each PDO time series with its corresponding estimate (4), and a are correlated at 0.7. On the other hand, CMIP5 ENSO2 forcing is generally greater than for the observations (Fig. 10c). These results indicate that the tropics–PDO linkage in the observations is different, both quantitatively and qualitatively, from most CMIP5 models, which may also be due to ENSO simulation errors (e.g., Bellenger et al. 2014; Capotondi et al. 2015). Also, note that most CMIP5 models overestimate r and underestimate the noise forcing, suggesting that mechanisms causing the

persistence of the PDO such as oceanic vertical mixing, SST reemergence, oceanic Rossby wave propagation, and/or ocean–atmosphere feedback in the midlatitudes play a stronger role in CMIP5 models than in the observations. Why these errors exist remains to be understood, but together they suggest that most CGCM PDOs may be more independent of the tropics than is observed.

5. Decadal-to-centennial PDO variability

As with simpler AR1 models, the LIM may be used to generate confidence intervals for power spectra, although

unlike simpler AR1 models, LIM-generated variability can include broadband spectral peaks (such as ENSO; Newman et al. 2009; Ault et al. 2013). Figure 11 shows that PDO spectra calculated from all four observational datasets (black lines) and, for the most part, the CMIP5 simulations (both control and historical) all generally lie within the LIM confidence intervals, quantified using 140 different 1750-yr realizations of (3) (e.g., Ault et al. 2013). So too do the 1000-yr, externally forced last millennium CMIP5 simulations that include estimates of explosive volcanism, solar variability, and anthropogenic changes to atmospheric composition and land use since 850, again suggesting that the PDO largely represents internal, unforced variability, even on decadal-to-centennial (or decen-) time scales. However, given that the CMIP5 PDO connections to the tropics are generally too weak and that unforced CMIP5 models generally underestimate decen tropical SST variability (Ault et al. 2013; Laepple and Huybers 2014), the agreement between the CMIP5 power spectra and the LIM may be somewhat fortuitous. That is, some “reddened ENSO” power in the observations is missing in the CMIP5 models, but its loss seems to be compensated for by too-persistent internally generated North Pacific SSTAs.

Even relative to a univariate AR1 (red noise) process, no statistically significant decadal or multidecadal peaks in these spectra are detectable (Pierce 2001). Rather, the PDO spectral power appears to continually increase with decreasing frequency f , raising the possibility that the spectra represent not red noise but rather long-memory, $1/f$ noise (Keshner 1982), with potentially pronounced regime behavior (e.g., Percival et al. 2001; Overland et al. 2006; Fleming 2014; see also Fraedrich et al. 2004). However, note that the LIM spectrum also is not flat over multidecadal time scales. In fact, spectral slopes are characteristic not only of some nonlinear systems but also aggregations of processes resulting from a multivariate AR1 system driven by noise (Milotti 1995; see also Penland and Sardeshmukh 2012).

Spectra for several paleoreconstructions of the PDO, made by combining proxies such as tree rings, corals, and sediments (Table 1), stay below the upper LIM confidence interval for decadal-to-multidecadal periods. Many of these reconstructions have been used to suggest the existence of PDO multidecadal spectral peaks, particularly for periods of about 20 and 70 yr (e.g., Biondi et al. 2001), although note that none of the observational datasets shows a significant peak on these time scales. However, poor reproducibility between the various PDO reconstructions (Fig. 11d) calls into question their collective fidelity as paleo-PDO indices, even for the multidecadal time scales that multicentury record lengths should be able to resolve (Fig. 11e). Beyond

profound differences in the various proxy networks used to reconstruct the PDO, the reconstructions also reflect differences in local climate variable responses to large-scale atmospheric and oceanic variability, potential seasonal biases, and geographic domain (e.g., Tingley et al. 2012; St. George 2014). As most PDO reconstructions are based on tree-ring-width time series, the statistical removal of biological growth-related trends in these series (Cook et al. 1995; Jones et al. 2009 and references therein) may deflate the centennial-scale variability, removing spectral power at the lowest frequencies in Fig. 11c.

Because the PDO represents not one but many dynamical processes, it poses a unique challenge as a target for proxy-based reconstruction. Thus far, reconstructions have largely sought to reproduce and extend the PDO index itself. A more nuanced approach that targets one or more of the different processes that contribute to PDO-related variability would likely lead to an understanding about how such processes have varied in the past, and their potential interrelationships. In pursuing such an approach, it is important to remember the different spectral biases in different proxy types; for example, some proxies could be strongly correlated with PDO-related variability simply because they are “climate integrators,” responding to ENSO-related forcing in the same way that the North Pacific Ocean does (Newman et al. 2003; see also Pederson et al. 2011). As it stands, the current disagreement among the existing PDO reconstructions is problematic for any assessment of PDO variability and PDO-related impacts over the last several hundred years (Kipfmüller et al. 2012).

6. Use of the PDO in climate diagnosis and prediction

In this section, we address both forecasting the PDO and forecasting with the PDO, focusing on the need to distinguish between PDO-correlated and PDO-predictable climate impacts.

a. Retrospective analysis of PDO impacts

PDO dependence on other climate processes implies that correlations with the PDO will be related to correlations with other climate indices. For example, Fig. 12 shows the correlation of revised U.S. climate division (nClimDiv; Vose et al. 2014) cold-season precipitation (left panels) and temperature (right panels) anomalies with the PDO, ENSO, and NPI indices. While there are some interesting differences, the precipitation maps are all quite similar, with ENSO having the most pronounced signal. For cold-season temperatures (Figs. 12d–f), there are notable differences between the PDO and ENSO

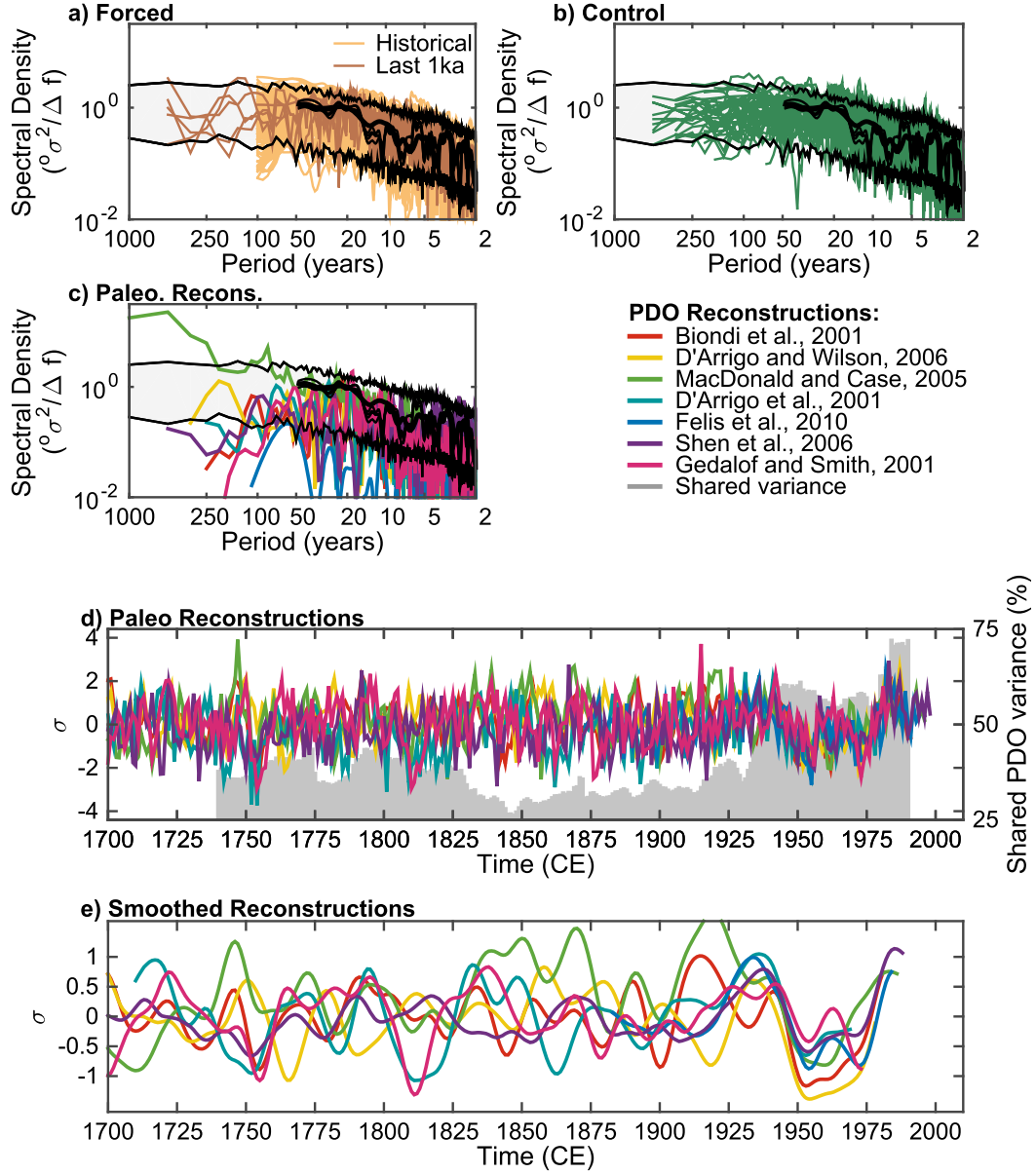


FIG. 11. Comparison of observed, paleoclimate, and CMIP5 PDO spectra: (a) CMIP5 historical simulations (190 runs total) and forced last millennium (past 1000 yr) simulations (6 runs), (b) unforced control simulations (48 runs total), and (c) paleoclimate (tree ring and other proxy based) reconstructions of the PDO. In (a)–(c), the thick black line represents the HadISST PDO spectrum, and the three thin black lines show the other three observational PDO spectra. In each case, only winter [November–March (NDJFM)] averages are used for consistency between data types. All PDO reconstruction indices were normalized to unit variance over 1901–2000; all other indices were normalized to the unit variance overall, not just the reference period. The gray shading and black lines show the upper and lower 95% confidence limits of the PDO power spectrum derived from 140 realizations of a LIM simulation [see (3)] each lasting 1750 yr. (d) Time series of each PDO reconstruction and the relative similarity of the reconstructions through time. The colored lines show the individual reconstructions themselves (left axis), while the gray shading shows the relative similarity (right axis), measured by the shared variance of the different indices through time, or the fraction of the total variance shared by all reconstructions in the correlation matrix of all time series over a moving 40-yr window. The ratio is computed by dividing the leading eigenvalue of the reconstruction correlation matrix by the total number of reconstructions available through time. (e) As in (d), but smoothed with a 21-yr running Gaussian filter.

TABLE 1. Paleoreconstructions of the PDO used in Fig. 11. Paleoclimate reconstructions were all obtained from the NOAA paleoclimatology program and are publicly available. Each of the PDO reconstructions targets slightly different aspects of the PDO, and each follows its own conventions for normalization, so all indices are normalized to unit variance over the period 1901–2000.

Reconstruction	Time period	Proxy used	Season targeted
Biondi et al. (2001)	1661–1991	Tree rings	Winter
D'Arrigo and Wilson (2006)	1565–1988	Tree rings	March–May (MAM)
Gedalof and Smith (2001)	1599–1983	Tree rings	MAM
MacDonald and Case (2005)	993–1996	Tree rings	Annual (January–December)
D'Arrigo et al. (2001)	1700–1979	Tree rings	Winter
Felis et al. (2010)	1873–1994	Coral (porites)	November–February (NDJF)
Shen et al. (2006)	1470–1998	Historical documents	Annual

correlation patterns; however, now the PDO pattern is quite similar to, and somewhat weaker than, the temperature correlations with the NPI. Since both ENSO and the NPI lead the PDO (Fig. 3), these results suggest that much of the PDO correlation patterns may not represent a direct response to the PDO. Repeating the analysis for the warm season (May–September) yields similar relationships between the correlation patterns, although all are somewhat weaker (not shown). A key concern then is to determine additional predictive information from the PDO, and not merely duplicate teleconnections from those processes that simultaneously act to force it.

Many studies that have explored historical PDO relationships with climate, especially hydrological quantities including precipitation, snowpack, streamflow, and drought (e.g., Gershunov and Barnett 1998; Hamlet and Lettenmaier 1999; McCabe and Dettinger 1999, 2002; Gutzler et al. 2002; Brown and Comrie 2004; McCabe et al. 2004; Stewart et al. 2005; Hunter et al. 2006; Kurtzman and Scanlon 2007; Yu and Zwiers 2007; Higgins et al. 2007; Hu and Huang 2009; Zhang et al. 2010; Goodrich and Walker 2011; Mehta et al. 2012; L. Li et al. 2012; McCabe et al. 2012; Cook et al. 2014; Oakley and Redmond 2014; Wang et al. 2014), are often focused on the impact of PDO phase on ENSO teleconnections. However, sorting ENSO responses by PDO phase may have unanticipated pitfalls beyond double counting the ENSO signal. On average, well over half of the large-scale extratropical atmospheric seasonal-mean anomaly occurring during an ENSO event is a consequence not of ENSO, but rather of ever-present weather and internal slowly evolving atmospheric anomalies such as blocking (e.g., Lau 1997). This “ENSO year but non-ENSO forced” atmospheric anomaly also modifies North Pacific SSTAs through changes in surface fluxes, while simultaneously contributing to the seasonal-mean climate anomaly downstream over North America (Pierce 2002). (Obviously, such anomalies exist in non-ENSO years as well, cf. NPI and PDO temperature correlations in Fig. 12.) Additionally, like snowflakes, no two ENSO

events are alike; recent research (see review by Capotondi et al. 2015) suggests that diversity among ENSO events may also drive different and/or asymmetric teleconnections across the North Pacific into North America (e.g., Hoerling et al. 2001; Larkin and Harrison 2005; Wu et al. 2005; Mo 2010; Yu et al. 2012). Of course, different teleconnections could drive variations in the atmospheric bridge with consequent PDO variations (e.g., An et al. 2007; Yeh et al. 2015), including on decadal time scales (Yeh and Kirtman 2008). ENSO diversity is evident in separate ENSO SST composites based on high and low PDO years (see Fig. 13; also cf. the North Pacific SSTAs for the two ENSO eigenmodes in Figs. 6d and 6f), raising the possibility that this stratification may partly capture ENSO diversity impacts on both PDO and ENSO teleconnections, rather than PDO impacts on ENSO teleconnections.

b. PDO prediction

Interest in PDO prediction is high due to its potential climate impacts, especially related to decadal variation and PDO regime shifts. From the earlier discussion, however, we might expect that predicting regime duration, which may depend upon the current amplitude of different processes with different memory time scales, could be more skillful than predicting regime shifts, which may be largely randomly forced.

Some extended forecast skill resulting from oceanic Rossby wave propagation (Schneider and Miller 2001) may occur for western Pacific SSTAs within the SAFZ. Recent studies established the multiyear predictability of the Kuroshio Extension speed (Nonaka et al. 2012; cf. Nonaka et al. 2016) and stability (Qiu et al. 2014) that enter the PDO forcing F in (1). How much this enhances PDO predictability (see Figs. 5a,b) remains to be determined, but it may be related to the more slowly evolving North Pacific component in Figs. 6a,b.

Given the PDO's relationship with ENSO, PDO forecast skill strongly depends on ENSO forecast skill, especially for forecast leads of up to 1–2 yr (e.g., Alexander et al. 2008; Wen et al. 2012). For longer

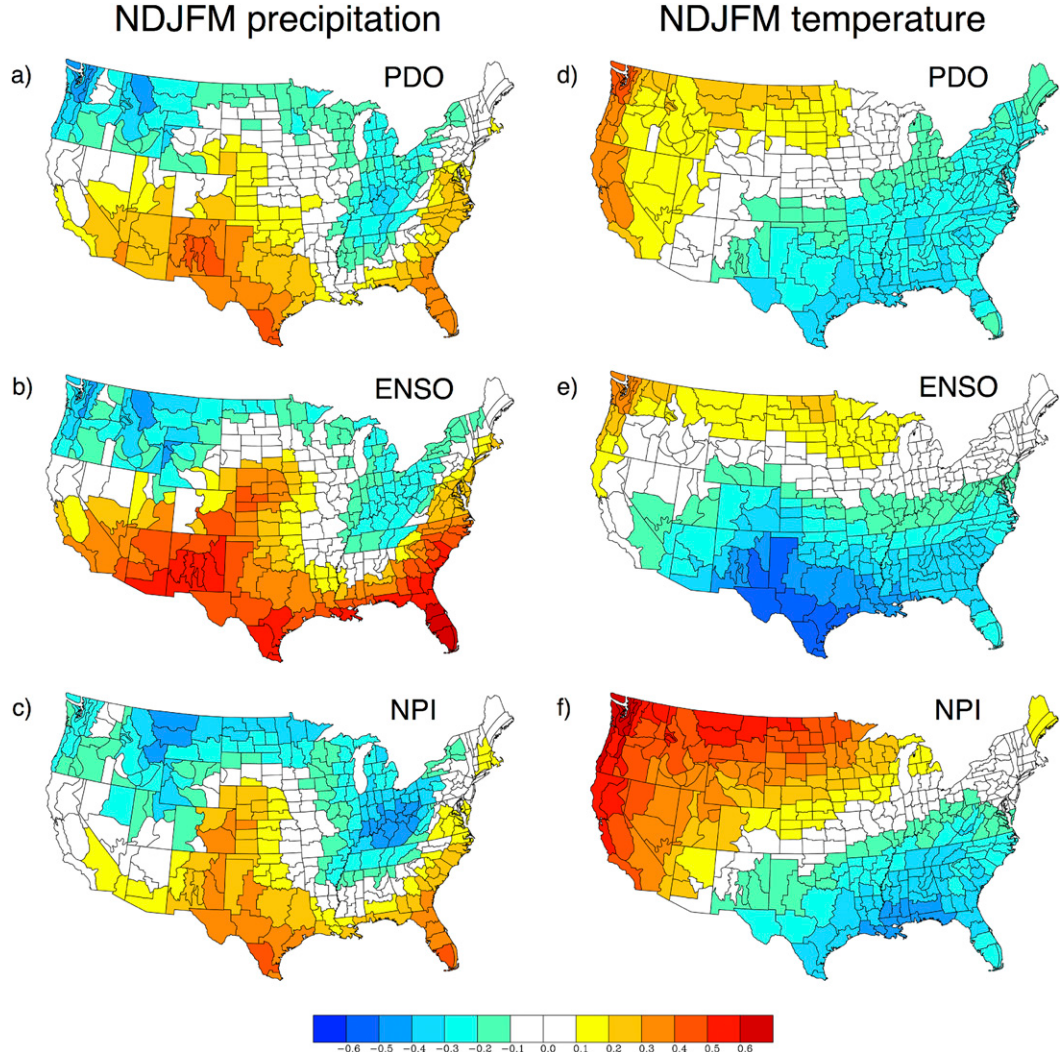


FIG. 12. Cold season relationship between climate indices discussed in this paper and U.S. precipitation and temperature anomalies determined from U.S. climate division data (Vose et al. 2014), for the years 1901–2014. NDJFM U.S. precipitation anomalies correlated with (a) the PDO index, (b) the ENSO index, and (c) the NPI. NDJFM U.S. temperature anomalies correlated with (d) the PDO index, (e) the ENSO index, and (f) the NPI.

forecast leads, largely unpredictable ENSO events act mostly as high-amplitude noise for decadal forecasts (Newman 2013; Wittenberg et al. 2014). This may help explain why decadal PDO forecast skill in CMIP5 hindcasts, which are initialized from the observed oceanic state, is unimpressive (Guemas et al. 2012; Kim et al. 2012; Van Oldenborgh et al. 2012; Newman 2013; Meehl and Teng 2014), although model bias also contributes (Guemas et al. 2012; Kim et al. 2014). Similarly, predicting the atmospheric impacts associated with the PDO may depend upon tropical forecast skill. In fact, current GCM forecasts initialized with a PDO SSTA alone have little atmospheric skill (Kumar et al. 2013; Kumar and Wang 2014), although additional skill

with higher-resolution models remains possible (e.g., Jung et al. 2012).

7. The IPO and the PDO

One particular pattern of ENSO-like decadal variability, the IPO (Power et al. 1999; Folland et al. 2002; Parker et al. 2007; Dai 2012), is often compared to the PDO. The precise definition of the IPO varies, but typically it has been defined as the projection of monthly Pacific SST data upon a pattern representing low-pass (~decadal) global SST variability (Parker et al. 2007; Henley et al. 2015). The resulting IPO monthly time series (Henley et al. 2015) is essentially

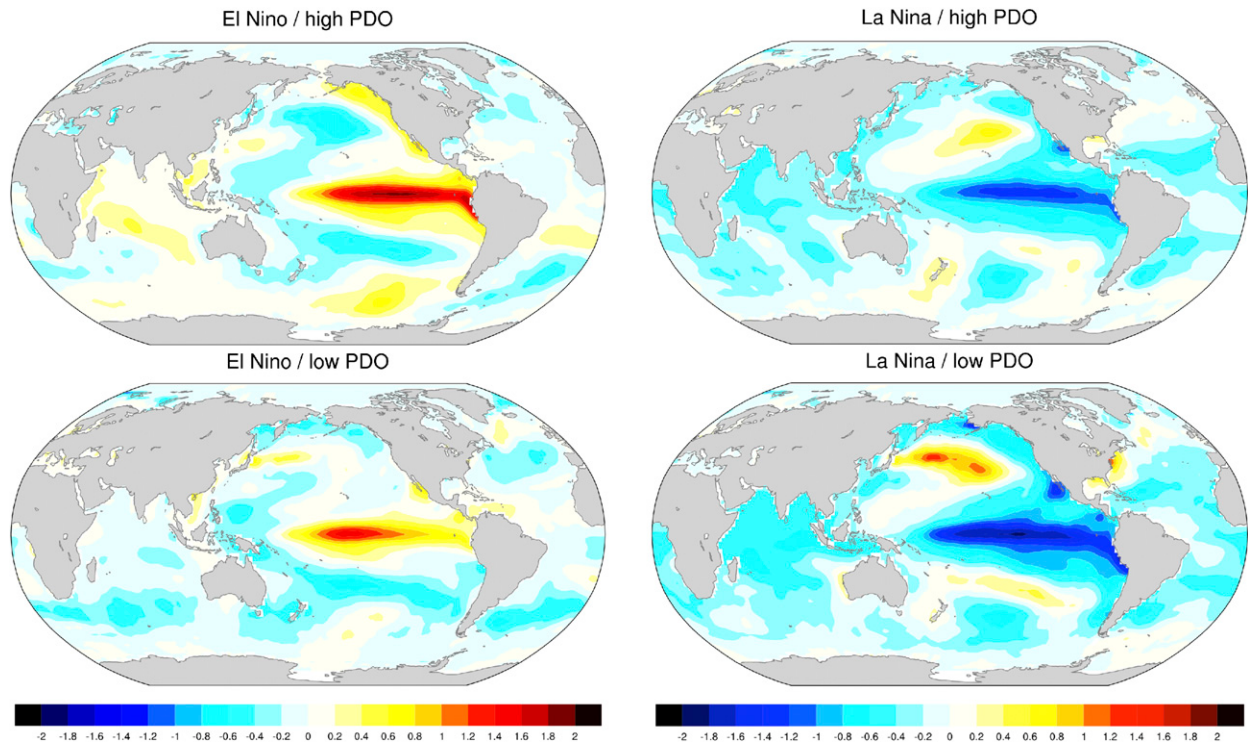


FIG. 13. NDJFM SST ENSO composites separated by high and low PDO values, determined over the years 1948–2008 from the ERSST.v3b SST dataset. Shown are composites of the top quintile (El Niño) of the ENSO index segregated by the (top left) top and (bottom left) the bottom halves of the PDO indices for the 12 cases, and the bottom quintile (La Niña) of the ENSO index segregated by the (top right) top and (bottom right) the bottom halves of the PDO indices for the 12 cases. Each half of the quintile is determined by ranking the PDO values of the quintile years. Contour interval is 0.2°C .

identical to the leading PC of the monthly Pacific basin SSTA variability, whether or not it has been low-pass filtered ($r = 0.99$). Moreover, the unfiltered IPO time series is very highly correlated to the ENSO PC used in Fig. 3 ($r = 0.96$), even when both are low-pass filtered ($r = 0.89$).

However, the IPO is not identical to the PDO. While North and South Pacific centers of action in the IPO regression pattern are roughly equivalent (e.g., Henley et al. 2015), the PDO North Pacific center is significantly enhanced (Fig. 1a; see also the orange circle in Fig. 2). Conversely, the South Pacific decadal oscillation (SPDO; e.g., Chen and Wallace 2015), the leading PC in the 20° – 70°S Pacific domain, has hemispheric asymmetry but with a South Pacific maximum in its regression pattern. The SPDO also has a reemergence (during austral spring) and stronger ENSO forcing (Shakun and Shaman 2009). In fact, the SPDO and IPO time series are actually more correlated ($r = 0.82$) than are the PDO and IPO time series ($r = 0.74$), although this difference diminishes with low-pass filtering. The PDO and SPDO unfiltered (low pass) PCs are also correlated, but less highly than each is to the IPO and ENSO, with $r = 0.5$ (0.56).

It seems reasonable to suggest, based on the above correlations as well as the discussion in sections 2 and 3,

that the IPO represents the reddened ENSO component, driven by both interannual and decadal ENSO variability, which is coherent between the North and South Pacific (Di Lorenzo et al. 2015). The difference between the PDO and IPO is then due to internal North Pacific processes, primarily because of atmospheric noise forcing of the PDO, directly through anomalous surface fluxes and indirectly via westward-propagating Rossby waves that drive SST variability in the SAFZ. Seasonality differences between the PDO and SPDO, in sensitivity to ENSO forcing and in reemergence, might also play a role in PDO–IPO differences, as would South Pacific atmospheric noise forcing. Which index should be used for climate diagnosis or prediction may thus depend upon the problem at hand. Note that the previous discussion relating to double counting in diagnostic studies will also apply (perhaps even more strongly) when using both ENSO and the IPO as predictors.

8. Concluding remarks

The PDO is now a well-established climate index, frequently used in correlation analyses to suggest physical linkage between a particular variable of

Summary View MECHANICS OF THE PACIFIC DECADAL OSCILLATION

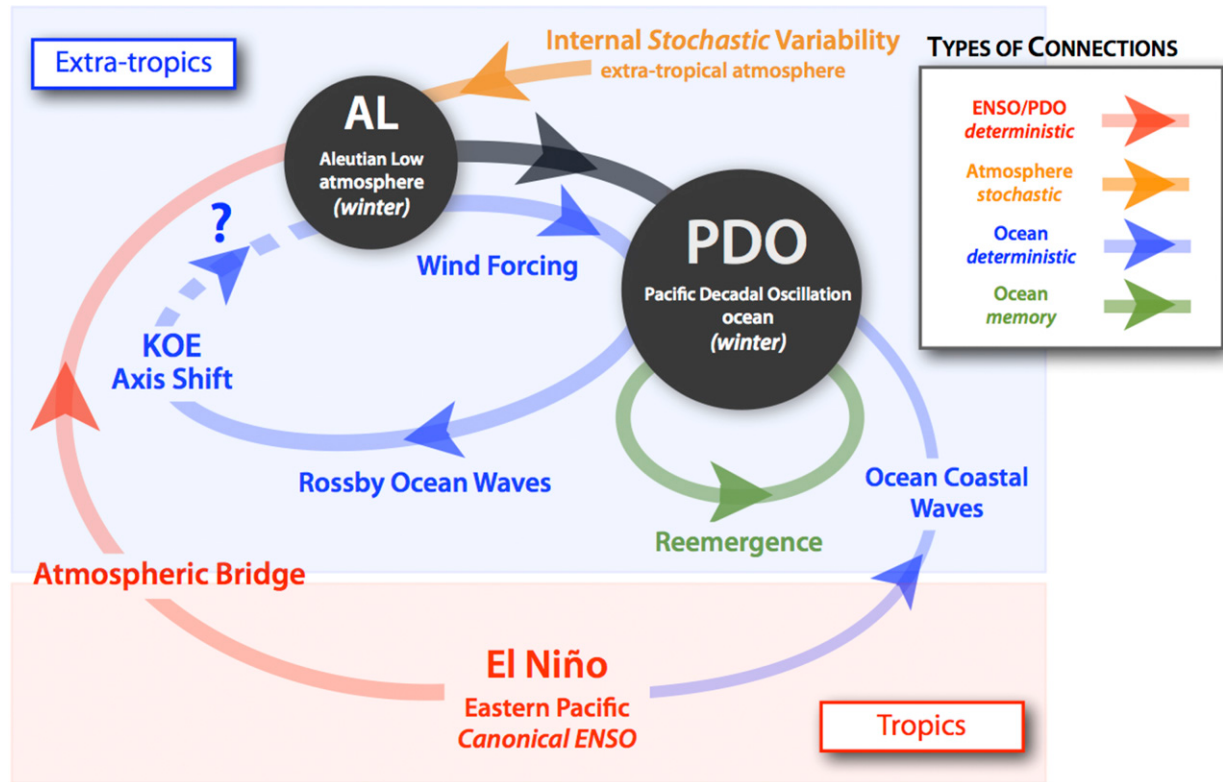


FIG. 14. Summary figure of the basic processes involved in the PDO.

interest and North Pacific Ocean variability. As summarized in Fig. 14, the PDO represents not a single phenomenon but rather a combination of processes that span the tropics and extratropics. It is therefore important to distinguish climate impacts *correlated* with the PDO from climate impacts that are *predictable* by the PDO. Within this context, since much of the PDO represents the oceanic response to atmospheric forcing, care should be taken when using the PDO as a “forcing function” of nonoceanic responses without a convincing argument for the physical forcing mechanism. For example, claiming that PDO drives contemporaneous changes in rainfall over western North America may be more simply explained by both variables (PDO and rainfall) being driven by a common forcing function (Pierce 2002) such as diverse ENSO events and the internal variability of the midlatitude atmosphere. A common forcing function must therefore be considered to be the first approximation for explaining a discovered simultaneous correlation between nonoceanic variables and PDO, including when reconstructing PDO-related variability into the past

with proxy records. Caution is also needed when using the PDO together with other indices in analyses where the PDO depends upon those indices; determining which portion of the PDO, and/or which PDO process, is legitimately an “independent” predictor is an important first step. Still, it is important to note that while the PDO is generally not an independent predictor, it also may not be assumed to be entirely dependent upon other predictors.

Ultimately, climate models may offer the best hope for establishing links with the PDO, because the historical record of PDO has limited degrees of freedom, a consequence of PDO representing an “integrated in time” response to forcing. Of course, the issues presented above still need consideration when analyzing model output. Moreover, while a realistic balance of PDO processes must be simulated in CGCMs, it appears that the current generation of models underestimates the tropical forcing of the PDO in the North Pacific Ocean. While models with particularly weak tropical-PDO connections could still be useful for examining some aspects of internal North Pacific Ocean dynamics

(e.g., [Zhong et al. 2008](#); [Giannakis and Majda 2012](#); [Zhang and Delworth 2015](#)) and possible feedback to the atmosphere ([Taguchi et al. 2012](#)), their inability to capture realistic tropical interactions with the North Pacific may yield problematic conclusions about the PDO and its role in the global climate system. In fact, [\(4\)](#) may provide a diagnostic foundation for process-based analysis of future CMIP6 CGCMs, since it tests not only how well ENSO variability is captured but also how ENSO teleconnections and North Pacific memory and dynamical processes are simulated.

This paper has focused on the PDO, but of course it is but one element of Pacific decadal variability (e.g., [Di Lorenzo et al. 2013, 2015](#)). Note that many of the caveats above should also be kept in mind when considering other modes in the North Pacific. We have only just begun to touch upon what this picture of the PDO as a sum of processes means for the diagnosis of PDO-related regional climate, ecological, and socioeconomic impacts; the reconstruction of the PDO and its multidecadal impacts from proxy data over the last several hundred years; and the relationship between the PDO and global mean temperature variations including the recent global surface warming “hiatus.” These issues will be explored in a forthcoming companion paper.

Acknowledgments. The authors wish to thank Mike Wallace, Mike McPhaden, Sasha Gershunov, Joe Barsugli, and an anonymous reviewer for helpful comments that significantly improved this paper. MN was supported by NOAA/CPO (CDEP) and NSF AGS CLD 1035325. MA and JDS acknowledge support from NOAA/CPO (ESM) and NASA. CD and ASP acknowledge support from the NOAA MAPP Program. NCAR is sponsored by the National Science Foundation. AJM was supported by NSF OCE1026607 and OCE1419306. SM and HN were supported in part by the Japanese Ministry of Education, Culture, Sports Science and Technology (MEXT) through Grant-in-Aid for Scientific Research 2205 in Innovative Areas. SM is also supported by JSPS KAKENHI Grants 15H01606, 26287110, and 26610146. HN is also supported by MEXT through Grants-in-Aid 25287120 and 26241003 and through Arctic Challenge for Sustainability Program, and by the Japanese Ministry of Environment through Environment Research and Technology Department Fund 2-1503. NS was supported by NSF1357015; U.S. Department of Energy, Office of Science, DOE-DESC000511; and JAMSTEC-IPRC Joint Investigations.

REFERENCES

- Alexander, M. A., 1990: Simulation of the response of the North Pacific Ocean to the anomalous atmospheric circulation associated with El Niño. *Climate Dyn.*, **5**, 53–65, doi:[10.1007/BF00195853](https://doi.org/10.1007/BF00195853).
- , 1992: Midlatitude atmosphere–ocean interaction during El Niño. Part I: The North Pacific Ocean. *J. Climate*, **5**, 944–958, doi:[10.1175/1520-0442\(1992\)005<0944:MAIDEN>2.0.CO;2](https://doi.org/10.1175/1520-0442(1992)005<0944:MAIDEN>2.0.CO;2).
- , 2010: Extratropical air–sea interaction, sea surface temperature variability, and the Pacific decadal oscillation. *Climate Dynamics: Why Does Climate Vary?*, *Geophys. Monogr.*, Vol. 189, Amer. Geophys. Union, 123–148.
- , and C. Deser, 1995: A mechanism for the recurrence of wintertime midlatitude SST anomalies. *J. Phys. Oceanogr.*, **25**, 122–137, doi:[10.1175/1520-0485\(1995\)025<0122:AMFTRO>2.0.CO;2](https://doi.org/10.1175/1520-0485(1995)025<0122:AMFTRO>2.0.CO;2).
- , and J. D. Scott, 2008: The role of Ekman ocean heat transport in the Northern Hemisphere response to ENSO. *J. Climate*, **21**, 5688–5707, doi:[10.1175/2008JCLI2382.1](https://doi.org/10.1175/2008JCLI2382.1).
- , C. Deser, and M. S. Timlin, 1999: The reemergence of SST anomalies in the North Pacific Ocean. *J. Climate*, **12**, 2419–2431, doi:[10.1175/1520-0442\(1999\)012<2419:TROSAI>2.0.CO;2](https://doi.org/10.1175/1520-0442(1999)012<2419:TROSAI>2.0.CO;2).
- , M. S. Timlin, and J. D. Scott, 2001: Winter-to-winter recurrence of sea surface temperature, salinity and mixed layer depth anomalies. *Prog. Oceanogr.*, **49**, 41–61, doi:[10.1016/S0079-6611\(01\)00015-5](https://doi.org/10.1016/S0079-6611(01)00015-5).
- , I. Bladé, M. Newman, J. R. Lanzante, N.-C. Lau, and J. D. Scott, 2002: The atmospheric bridge: The influence of ENSO teleconnections on air–sea interaction over the global oceans. *J. Climate*, **15**, 2205–2231, doi:[10.1175/1520-0442\(2002\)015<2205:TABTIO>2.0.CO;2](https://doi.org/10.1175/1520-0442(2002)015<2205:TABTIO>2.0.CO;2).
- , N.-C. Lau, and J. D. Scott, 2004: Broadening the atmospheric bridge paradigm: ENSO teleconnections to the North Pacific in summer and to the tropical west Pacific–Indian Oceans over the seasonal cycle. *Earth’s Climate: The Ocean–Atmosphere Interaction*, *Geophys. Monogr.*, Vol. 147, 85–104.
- , L. Matrosova, C. Penland, J. D. Scott, and P. Chang, 2008: Forecasting Pacific SSTs: Linear inverse model predictions of the PDO. *J. Climate*, **21**, 385–402, doi:[10.1175/2007JCLI1849.1](https://doi.org/10.1175/2007JCLI1849.1).
- , D. J. Vimont, P. Chang, and J. D. Scott, 2010: The impact of extratropical atmospheric variability on ENSO: Testing the seasonal footprinting mechanism using coupled model experiments. *J. Climate*, **23**, 2885–2901, doi:[10.1175/2010JCLI3205.1](https://doi.org/10.1175/2010JCLI3205.1).
- An, S. I., J.-S. Kug, A. Timmermann, I.-S. Kang, and O. Timm, 2007: The influence of ENSO on the generation of decadal variability in the North Pacific. *J. Climate*, **20**, 667–680, doi:[10.1175/JCLI4017.1](https://doi.org/10.1175/JCLI4017.1).
- Ault, T., C. Deser, M. Newman, and J. Emile-Geay, 2013: Characterizing decadal to centennial variability in the equatorial Pacific during the last millennium. *Geophys. Res. Lett.*, **40**, 3450–3456, doi:[10.1002/grl.50647](https://doi.org/10.1002/grl.50647).
- Baines, P. G., and C. K. Folland, 2007: Evidence for a rapid global climate shift across the late 1960s. *J. Climate*, **20**, 2721–2744, doi:[10.1175/JCLI4177.1](https://doi.org/10.1175/JCLI4177.1).
- Balmaseda, M. A., K. Mogensen, and A. T. Weaver, 2013: Evaluation of the ECMWF ocean reanalysis system ORAS4. *Quart. J. Roy. Meteor. Soc.*, **139**, 1132–1161, doi:[10.1002/qj.2063](https://doi.org/10.1002/qj.2063).
- Barlow, M., S. Nigam, and E. H. Berbery, 2001: ENSO, Pacific decadal variability, and U.S. summertime precipitation, drought, and stream flow. *J. Climate*, **14**, 2105–2128, doi:[10.1175/1520-0442\(2001\)014<2105:EPDVAU>2.0.CO;2](https://doi.org/10.1175/1520-0442(2001)014<2105:EPDVAU>2.0.CO;2).
- Barnett, T., D. W. Pierce, M. Latif, D. Domonget, and R. Saravanan, 1999: Interdecadal interactions between the tropics and the midlatitudes in the Pacific basin. *Geophys. Res. Lett.*, **26**, 615–618, doi:[10.1029/1999GL900042](https://doi.org/10.1029/1999GL900042).

- Barsugli, J. J., and D. S. Battisti, 1998: The basic effects of atmosphere–ocean thermal coupling on midlatitude variability. *J. Atmos. Sci.*, **55**, 477–493, doi:10.1175/1520-0469(1998)055<0477:TBEAOA>2.0.CO;2.
- Bellenger, H., É. Guilyardi, J. Leloup, M. Lengaigne, and J. Vialard, 2014: ENSO representation in climate models: From CMIP3 to CMIP5. *Climate Dyn.*, **42**, 1999–2018, doi:10.1007/s00382-013-1783-z.
- Beran, J., 1994: *Statistics for Long-Memory Processes*. Chapman and Hall, 315 pp.
- Bhatt, U. S., M. A. Alexander, D. S. Battisti, D. D. Houghton, and L. M. Keller, 1998: Atmosphere–ocean interaction in the North Atlantic: Near-surface climate variability. *J. Climate*, **11**, 1615–1632, doi:10.1175/1520-0442(1998)011<1615:AOITN>2.0.CO;2.
- Biondi, F., A. Gershunov, and D. R. Cayan, 2001: North Pacific decadal climate variability since 1661. *J. Climate*, **14**, 5–10, doi:10.1175/1520-0442(2001)014<0005:NPDCVS>2.0.CO;2.
- Bladé, I., 1997: The influence of midlatitude coupling on the low-frequency variability of a GCM. Part I: No tropical SST forcing. *J. Climate*, **10**, 2087–2106, doi:10.1175/1520-0442(1997)010<2087:TIOMOA>2.0.CO;2.
- Bond, N. A., J. E. Overland, M. Spillane, and P. Stabeno, 2003: Recent shifts in the state of the North Pacific. *Geophys. Res. Lett.*, **30**, 2183, doi:10.1029/2003GL018597.
- Brown, D. P., and A. C. Comrie, 2004: A winter precipitation “dipole” in the western United States associated with multi-decadal ENSO variability. *Geophys. Res. Lett.*, **31**, L09203, doi:10.1029/2003GL018726.
- Capotondi, A., M. A. Alexander, and C. Deser, 2003: Why are there Rossby wave maxima at 10°S and 13°N in the Pacific? *J. Phys. Oceanogr.*, **33**, 1549–1563, doi:10.1175/2407.1.
- , —, —, and M. McPhaden, 2005: Anatomy and decadal evolution of the Pacific subtropical cells. *J. Climate*, **18**, 3739–3758, doi:10.1175/JCLI3496.1.
- , —, and Coauthors, 2015: Understanding ENSO diversity. *Bull. Amer. Meteor. Soc.*, **96**, 921–938, doi:10.1175/BAMS-D-13-00117.1.
- Carton, J. A., and B. S. Giese, 2008: A reanalysis of ocean climate using Simple Ocean Data Assimilation (SODA). *Mon. Wea. Rev.*, **136**, 2999–3017, doi:10.1175/2007MWR1978.1.
- Cayan, D. R., 1992: Latent and sensible heat flux anomalies over the northern oceans: The connection to monthly atmospheric circulation. *J. Climate*, **5**, 354–369, doi:10.1175/1520-0442(1992)005<0354:LASHFA>2.0.CO;2.
- Chelton, D. B., and R. E. Davis, 1982: Monthly mean sea level variability along the west coast of North America. *J. Phys. Oceanogr.*, **12**, 757–784, doi:10.1175/1520-0485(1982)012<0757:MMSLVA>2.0.CO;2.
- Chen, X. Y., and J. M. Wallace, 2015: ENSO-like variability: 1900–2013. *J. Climate*, **28**, 9623–9641, doi:10.1175/JCLI-D-15-0322.1.
- Chiang, J. C. H., and D. J. Vimont, 2004: Analogous meridional modes of atmosphere–ocean variability in the tropical Pacific and tropical Atlantic. *J. Climate*, **17**, 4143–4158, doi:10.1175/JCLI4953.1.
- Clarke, A. J., and S. Van Gorder, 1994: On ENSO coastal currents and sea levels. *J. Phys. Oceanogr.*, **24**, 661–680, doi:10.1175/1520-0485(1994)024<0661:OECCAS>2.0.CO;2.
- Clement, A. C., R. Burgman, and J. R. Norris, 2009: Observational and model evidence for positive low-level cloud feedback. *Science*, **325**, 460–464, doi:10.1126/science.1171255.
- Compo, G., and P. D. Sardeshmukh, 2010: Removing ENSO-related variations from the climate record. *J. Climate*, **23**, 1957–1978, doi:10.1175/2009JCLI2735.1.
- Cook, B. I., J. E. Smerdon, R. Seager, and E. R. Cook, 2014: Pan-continental droughts in North America over the last millennium. *J. Climate*, **27**, 383–397, doi:10.1175/JCLI-D-13-00100.1.
- Cook, E. R., K. R. Briffa, D. M. Meko, D. A. Graybill, and G. Funkhouser, 1995: The segment length curse in long tree-ring chronology development for paleoclimatic studies. *Holocene*, **5**, 229–237, doi:10.1177/095968369500500211.
- Dai, A., 2012: The influence of the inter-decadal Pacific oscillation on US precipitation during 1923–2010. *Climate Dyn.*, **41**, 633–646, doi:10.1007/s00382-012-1446-5.
- D’Arrigo, R., and R. Wilson, 2006: On the Asian expression of the PDO. *Int. J. Climatol.*, **26**, 1607–1617, doi:10.1002/joc.1326.
- , R. Villalba, and G. Wiles, 2001: Tree-ring estimates of Pacific decadal climate variability. *Climate Dyn.*, **18**, 219–224, doi:10.1007/s003820100177.
- Davis, R. E., 1976: Predictability of sea surface temperature and sea level pressure anomalies over the North Pacific Ocean. *J. Phys. Oceanogr.*, **6**, 249–266, doi:10.1175/1520-0485(1976)006<0249:POSSTA>2.0.CO;2.
- Deser, C., and M. L. Blackmon, 1995: On the relationship between tropical and North Pacific sea surface temperature variations. *J. Climate*, **8**, 1677–1680, doi:10.1175/1520-0442(1995)008<1677:OTRBTA>2.0.CO;2.
- , and M. Timlin, 1997: Atmosphere–ocean interaction on weekly timescales in the North Atlantic and Pacific. *J. Climate*, **10**, 393–408, doi:10.1175/1520-0442(1997)010<0393:AOIOWT>2.0.CO;2.
- , M. A. Alexander, and M. S. Timlin, 1996: Upper-ocean thermal variations in the North Pacific during 1970–1991. *J. Climate*, **9**, 1840–1855, doi:10.1175/1520-0442(1996)009<1840:UOTVIT>2.0.CO;2.
- , —, and —, 1999: Evidence for wind-driven intensification of the Kuroshio Current Extension from the 1970s to the 1980s. *J. Climate*, **12**, 1697–1706, doi:10.1175/1520-0442(1999)012<1697:EFAWDI>2.0.CO;2.
- , —, and —, 2003: Understanding the persistence of sea surface temperature anomalies in midlatitudes. *J. Climate*, **16**, 57–72, doi:10.1175/1520-0442(2003)016<0057:UTPOSS>2.0.CO;2.
- , A. S. Phillips, and J. W. Hurrell, 2004: Pacific interdecadal climate variability: Linkages between the tropics and the North Pacific during boreal winter since 1900. *J. Climate*, **17**, 3109–3124, doi:10.1175/1520-0442(2004)017<3109:PICVLB>2.0.CO;2.
- , and Coauthors, 2012: ENSO and Pacific decadal variability in the Community Climate System Model version 4. *J. Climate*, **25**, 2622–2651, doi:10.1175/JCLI-D-11-00301.1.
- Di Lorenzo, E., and Coauthors, 2008: North Pacific gyre oscillation links ocean climate and ecosystem change. *Geophys. Res. Lett.*, **35**, L08607, doi:10.1029/2007GL032838.
- , K. M. Cobb, J. C. Furtado, N. Schneider, B. T. Anderson, A. Bracco, M. A. Alexander, and D. J. Vimont, 2010: Central Pacific El Niño and decadal climate change in the North Pacific. *Nat. Geosci.*, **3**, 762–765, doi:10.1038/ngeo984.
- , and Coauthors, 2013: Synthesis of Pacific Ocean climate and ecosystem dynamics. *Oceanography*, **26**, 68–81, doi:10.5670/oceanog.2013.76.
- , G. Liguori, N. Schneider, J. C. Furtado, B. T. Anderson, and M. A. Alexander, 2015: ENSO and meridional modes: A null

- hypothesis for Pacific climate variability. *Geophys. Res. Lett.*, **42**, 9440–9448, doi:[10.1002/2015gl066281](https://doi.org/10.1002/2015gl066281).
- Ebbesmeyer, C. C., D. R. Cayan, D. R. McLain, F. H. Nichols, D. H. Peterson, and K. T. Redmond, 1991: 1976 step in the Pacific climate: Forty environmental changes between 1968–1975 and 1977–1985. *Proc. Seventh Annual Pacific Climate Workshop*, Asilomar, CA, California Dept. of Water Research, 115–126. [Available online at http://aquaticcommons.org/4562/1/EbbesmeyerEtal_1990_ProcPacCLIM7th_pp115-126.pdf.]
- Enfield, D. B., and J. S. Allen, 1980: On the structure and dynamics of monthly mean sea level anomalies along the Pacific coast of North and South America. *J. Phys. Oceanogr.*, **10**, 557–588, doi:[10.1175/1520-0485\(1980\)010<0557:OTSADO>2.0.CO;2](https://doi.org/10.1175/1520-0485(1980)010<0557:OTSADO>2.0.CO;2).
- Felis, T., A. Suzuki, H. Kuhnert, N. Rimbu, and H. Kawahata, 2010: Pacific decadal oscillation documented in a coral record of North Pacific winter temperature since 1873. *Geophys. Res. Lett.*, **37**, L14605, doi:[10.1029/2010GL043572](https://doi.org/10.1029/2010GL043572).
- Fleming, S. W., 2009: Exploring the nature of Pacific climate variability using a “toy” nonlinear stochastic model. *Can. J. Phys.*, **87**, 1127–1131, doi:[10.1139/P09-095](https://doi.org/10.1139/P09-095).
- , 2014: A non-uniqueness problem in the identification of power-law spectral scaling for hydroclimatic time series. *Hydrolog. Sci. J.*, **59**, 73–84, doi:[10.1080/02626667.2013.851384](https://doi.org/10.1080/02626667.2013.851384).
- Folland, C. K., J. A. Renwick, M. J. Salinger, and A. B. Mullan, 2002: Relative influences of the interdecadal Pacific oscillation and ENSO on the South Pacific convergence zone. *Geophys. Res. Lett.*, **29**, 1643, doi:[10.1029/2001GL014201](https://doi.org/10.1029/2001GL014201).
- Fraedrich, K., U. Luksch, and R. Blender, 2004: 1/f model for long-time memory of the ocean surface temperature. *Phys. Rev. E*, **70**, 037301, doi:[10.1103/PhysRevE.70.037301](https://doi.org/10.1103/PhysRevE.70.037301).
- Frankignoul, C., 1999: A cautionary note on the use of statistical atmospheric models in the middle latitudes: Comments on “Decadal variability in the North Pacific as simulated by a hybrid coupled model.” *J. Climate*, **12**, 1871–1872, doi:[10.1175/1520-0442\(1999\)012<1871:ACNOTU>2.0.CO;2](https://doi.org/10.1175/1520-0442(1999)012<1871:ACNOTU>2.0.CO;2).
- , and K. Hasselmann, 1977: Stochastic climate models. Part II: Application to sea-surface temperature anomalies and thermocline variability. *Tellus*, **29**, 289–305, doi:[10.1111/j.2153-3490.1977.tb00740.x](https://doi.org/10.1111/j.2153-3490.1977.tb00740.x).
- , and R. W. Reynolds, 1983: Testing a dynamical model for mid-latitude sea surface temperature anomalies. *J. Phys. Oceanogr.*, **13**, 1131–1145, doi:[10.1175/1520-0485\(1983\)013<1131:TADMF>2.0.CO;2](https://doi.org/10.1175/1520-0485(1983)013<1131:TADMF>2.0.CO;2).
- , P. Müller, and E. Zorita, 1997: A simple model of the decadal response of the ocean to stochastic wind forcing. *J. Phys. Oceanogr.*, **27**, 1533–1546, doi:[10.1175/1520-0485\(1997\)027<1533:ASMOTD>2.0.CO;2](https://doi.org/10.1175/1520-0485(1997)027<1533:ASMOTD>2.0.CO;2).
- , N. Sennechael, Y. Kwon, and M. Alexander, 2011: Influence of the meridional shifts of the Kuroshio and the Oyashio Extensions on the atmospheric circulation. *J. Climate*, **24**, 762–777, doi:[10.1175/2010JCLI3731.1](https://doi.org/10.1175/2010JCLI3731.1).
- Furtado, J. C., E. Di Lorenzo, N. Schneider, and N. A. Bond, 2011: North Pacific decadal variability and climate change in the IPCC AR4 models. *J. Climate*, **24**, 3049–3067, doi:[10.1175/2010JCLI3584.1](https://doi.org/10.1175/2010JCLI3584.1).
- Gedalof, Z., and D. J. Smith, 2001: Interdecadal climate variability and regime-scale shifts in Pacific North America. *Geophys. Res. Lett.*, **28**, 1515–1518, doi:[10.1029/2000GL011779](https://doi.org/10.1029/2000GL011779).
- Gershunov, A., and T. P. Barnett, 1998: Interdecadal modulation of ENSO teleconnections. *Bull. Amer. Meteor. Soc.*, **79**, 2715–2725, doi:[10.1175/1520-0477\(1998\)079<2715:IMOET>2.0.CO;2](https://doi.org/10.1175/1520-0477(1998)079<2715:IMOET>2.0.CO;2).
- Giannakis, D., and A. J. Majda, 2012: Limits of predictability in the North Pacific sector of a comprehensive climate model. *Geophys. Res. Lett.*, **39**, L24602, doi:[10.1029/2012GL054273](https://doi.org/10.1029/2012GL054273).
- Gill, A. E., 1982: *Atmosphere–Ocean Dynamics*. Academic Press, 662 pp.
- Goodrich, G. B., and J. M. Walker, 2011: The influence of the PDO on winter precipitation during high- and low-index ENSO conditions in the eastern United States. *Phys. Geogr.*, **32**, 295–312, doi:[10.2747/0272-3646.32.4.295](https://doi.org/10.2747/0272-3646.32.4.295).
- Graham, N. E., 1994: Decadal-scale climate variability in the 1970s and 1980s: Observations and model results. *Climate Dyn.*, **10**, 135–159, doi:[10.1007/BF00210626](https://doi.org/10.1007/BF00210626).
- Granger, C. W. J., 1980: Long memory relationships and the aggregation of dynamic models. *J. Econom.*, **14**, 227–238, doi:[10.1016/0304-4076\(80\)90092-5](https://doi.org/10.1016/0304-4076(80)90092-5).
- Gu, D., and S. G. H. Philander, 1997: Interdecadal climate fluctuations that depend on exchanges between the tropics and extratropics. *Science*, **275**, 805–807, doi:[10.1126/science.275.5301.805](https://doi.org/10.1126/science.275.5301.805).
- Guan, B., and S. Nigam, 2008: Pacific sea surface temperatures in the twentieth century: An evolution-centric analysis of variability and trend. *J. Climate*, **21**, 2790–2809, doi:[10.1175/2007JCLI2076.1](https://doi.org/10.1175/2007JCLI2076.1).
- Guemas, V., F. J. Doblas-Reyes, F. Liennert, Y. Soufflet, and H. Du, 2012: Identifying the causes of the poor decadal climate prediction skill over the North Pacific. *J. Geophys. Res.*, **117**, D20111, doi:[10.1029/2012JD018004](https://doi.org/10.1029/2012JD018004).
- Gutzler, D. S., D. M. Kann, and C. Thorncroft, 2002: Modulation of ENSO-based long-lead outlooks of southwestern U.S. winter precipitation by the Pacific decadal oscillation. *Wea. Forecasting*, **17**, 1163–1172, doi:[10.1175/1520-0434\(2002\)017<1163:MOEBLL>2.0.CO;2](https://doi.org/10.1175/1520-0434(2002)017<1163:MOEBLL>2.0.CO;2).
- Hamlet, A. F., and D. P. Lettenmaier, 1999: Columbia River streamflow forecasting based on ENSO and PDO climate signals. *J. Water Res. Plann. Manage.*, **125**, 333–341, doi:[10.1061/\(ASCE\)0733-9496\(1999\)125:6\(333\)](https://doi.org/10.1061/(ASCE)0733-9496(1999)125:6(333)).
- Hanawa, K., and S. Sugimoto, 2004: ‘Reemergence’ areas of winter sea surface temperature anomalies in the world’s oceans. *Geophys. Res. Lett.*, **31**, L10303, doi:[10.1029/2004GL019904](https://doi.org/10.1029/2004GL019904).
- Hasselmann, K., 1976: Stochastic climate models. Part I. Theory. *Tellus*, **28**, 473–485, doi:[10.1111/j.2153-3490.1976.tb00696.x](https://doi.org/10.1111/j.2153-3490.1976.tb00696.x).
- Henley, B. J., J. Gergis, D. J. Karoly, S. B. Power, J. Kennedy, and C. K. Folland, 2015: A tripole index for the interdecadal Pacific oscillation. *Climate Dyn.*, **45**, 3077–3090, doi:[10.1007/s00382-015-2525-1](https://doi.org/10.1007/s00382-015-2525-1).
- Higgins, R. W., V. B. S. Silva, W. Shi, and J. Larson, 2007: Relationships between climate variability and fluctuations in daily precipitation over the United States. *J. Climate*, **20**, 3561–3579, doi:[10.1175/JCLI4196.1](https://doi.org/10.1175/JCLI4196.1).
- Hoerling, M. P., A. Kumar, and T. Xu, 2001: Robustness of the non-linear climate response to ENSO’s extreme phases. *J. Climate*, **14**, 1277–1293, doi:[10.1175/1520-0442\(2001\)014<1277:ROTNCR>2.0.CO;2](https://doi.org/10.1175/1520-0442(2001)014<1277:ROTNCR>2.0.CO;2).
- Hsieh, C.-H., S. M. Glaser, A. J. Lucas, and G. Sugihara, 2005: Distinguishing random environmental fluctuations from ecological catastrophes for the North Pacific Ocean. *Nature*, **435**, 336–340, doi:[10.1038/nature03553](https://doi.org/10.1038/nature03553).
- Hu, Z.-Z., and B. Huang, 2009: Interferential impact of ENSO and PDO on dry and wet conditions in the U.S. Great Plains. *J. Climate*, **22**, 6047–6065, doi:[10.1175/2009JCLI2798.1](https://doi.org/10.1175/2009JCLI2798.1).
- Hunter, T., G. Tootle, and T. Piechota, 2006: Oceanic–atmospheric variability and western U.S. snowfall. *Geophys. Res. Lett.*, **33**, L13706, doi:[10.1029/2006GL026600](https://doi.org/10.1029/2006GL026600).

- Ishii, M., A. Shouji, S. Sugimoto, and T. Matsumoto, 2005: Objective analyses of sea-surface temperature and marine meteorological variables for the 20th century using ICOADS and the Kobe Collection. *Int. J. Climatol.*, **25**, 865–879, doi:[10.1002/joc.1169](https://doi.org/10.1002/joc.1169).
- Iwasaka, N., and J. M. Wallace, 1995: Large scale air sea interaction in the Northern Hemisphere from a view point of variations of surface heat flux by SVD analysis. *J. Meteor. Soc. Japan*, **73**, 781–794.
- Jones, P. D., and Coauthors, 2009: High-resolution paleoclimatology of the last millennium: A review of current status and future prospects. *Holocene*, **19**, 3–49, doi:[10.1177/0959683608098952](https://doi.org/10.1177/0959683608098952).
- Jung, T., and Coauthors, 2012: High-resolution global climate simulations with the ECMWF model in Project Athena: Experimental design, model climate, and seasonal forecast skill. *J. Climate*, **25**, 3155–3172, doi:[10.1175/JCLI-D-11-00265.1](https://doi.org/10.1175/JCLI-D-11-00265.1).
- Kaplan, A., M. Cane, Y. Kushnir, A. Clement, M. Blumenthal, and B. Rajagopalan, 1998: Analyses of global sea surface temperature 1856–1991. *J. Geophys. Res.*, **103**, 18 567–18 589, doi:[10.1029/97JC01736](https://doi.org/10.1029/97JC01736).
- Kay, J. E., and Coauthors, 2015: The Community Earth System Model (CESM) Large Ensemble Project: A community resource for studying climate change in the presence of internal climate variability. *Bull. Amer. Meteor. Soc.*, **96**, 1333–1349, doi:[10.1175/BAMS-D-13-00255.1](https://doi.org/10.1175/BAMS-D-13-00255.1).
- Kelly, K. A., R. J. Small, R. M. Samelson, B. Qiu, T. M. Joyce, Y.-O. Kwon, and M. F. Cronin, 2010: Western boundary currents and frontal air-sea interaction: Gulf Stream and Kuroshio Extension. *J. Climate*, **23**, 5644–5667, doi:[10.1175/2010JCLI3346.1](https://doi.org/10.1175/2010JCLI3346.1).
- Keshner, M. S., 1982: 1/f noise. *Proc. IEEE*, **70**, 212, doi:[10.1109/PROC.1982.12282](https://doi.org/10.1109/PROC.1982.12282).
- Kim, H.-M., P. J. Webster, and J. A. Curry, 2012: Evaluation of short-term climate change prediction in multi-model CMIP5 decadal hindcasts. *Geophys. Res. Lett.*, **39**, L10701, doi:[10.1029/2012GL051644](https://doi.org/10.1029/2012GL051644).
- , Y. G. Ham, and A. A. Scaife, 2014: Improvement of initialized decadal predictions over the North Pacific Ocean by systematic anomaly pattern correction. *J. Climate*, **27**, 5148–5162, doi:[10.1175/JCLI-D-13-00519.1](https://doi.org/10.1175/JCLI-D-13-00519.1).
- Kipfmüller, K. F., E. R. Larson, and S. St. George, 2012: Does proxy uncertainty affect the relations inferred between the Pacific decadal oscillation and wildfire activity in the western United States? *Geophys. Res. Lett.*, **39**, L04703, doi:[10.1029/2011GL050645](https://doi.org/10.1029/2011GL050645).
- Kleeman, R., J. P. McCreary, and B. A. Klinger, 1999: A mechanism for the decadal variation of ENSO. *Geophys. Res. Lett.*, **26**, 1743–1747, doi:[10.1029/1999GL900352](https://doi.org/10.1029/1999GL900352).
- Klein, S. A., D. L. Hartmann, and J. R. Norris, 1995: On the relationships among low-cloud structure, sea surface temperature, and atmospheric circulation in the summertime northeast Pacific. *J. Climate*, **8**, 1140–1155, doi:[10.1175/1520-0442\(1995\)008<1140:OTRALC>2.0.CO;2](https://doi.org/10.1175/1520-0442(1995)008<1140:OTRALC>2.0.CO;2).
- Kumar, A., and H. Wang, 2014: On the potential of extratropical SST anomalies for improving climate predictions. *Climate Dyn.*, **44**, 2557–2569, doi:[10.1007/s00382-014-2398-8](https://doi.org/10.1007/s00382-014-2398-8).
- , —, W. Wang, Y. Xue, and Z.-Z. Hu, 2013: Does knowing the oceanic PDO phase help predict the atmospheric anomalies in subsequent months? *J. Climate*, **26**, 1268–1285, doi:[10.1175/JCLI-D-12-00057.1](https://doi.org/10.1175/JCLI-D-12-00057.1).
- Kurtzman, D., and B. R. Scanlon, 2007: El Niño–Southern Oscillation and Pacific decadal oscillation impacts on precipitation in the southern and central United States: Evaluation of spatial distribution and predictions. *Water Resour. Res.*, **43**, W10427, doi:[10.1029/2007WR005863](https://doi.org/10.1029/2007WR005863).
- Kushnir, Y., W. A. Robinson, I. Bladé, N. M. J. Hall, S. Peng, and R. Sutton, 2002: Atmospheric GCM response to extratropical SST anomalies: Synthesis and evaluation. *J. Climate*, **15**, 2233–2256, doi:[10.1175/1520-0442\(2002\)015<2233:AGRTES>2.0.CO;2](https://doi.org/10.1175/1520-0442(2002)015<2233:AGRTES>2.0.CO;2).
- Kwon, Y.-O., and C. Deser, 2007: North Pacific decadal variability in the Community Climate System Model version 2. *J. Climate*, **20**, 2416–2433, doi:[10.1175/JCLI4103.1](https://doi.org/10.1175/JCLI4103.1).
- , M. A. Alexander, N. A. Bond, C. Frankignoul, H. Nakamura, B. Qiu, and L. A. Thompson, 2010a: Role of the Gulf Stream and Kuroshio–Oyashio systems in large-scale atmosphere–ocean interaction: A review. *J. Climate*, **23**, 3249–3281, doi:[10.1175/2010JCLI3343.1](https://doi.org/10.1175/2010JCLI3343.1).
- , C. Deser, and C. Cassou, 2010b: Coupled atmosphere–mixed layer ocean response to ocean heat flux convergence along the Kuroshio Current Extension. *Climate Dyn.*, **36**, 2295–2312, doi:[10.1007/s00382-010-0764-8](https://doi.org/10.1007/s00382-010-0764-8).
- Laepple, T., and P. Huybers, 2014: Global and regional variability in marine surface temperatures. *Geophys. Res. Lett.*, **41**, 2528–2534, doi:[10.1002/2014GL059345](https://doi.org/10.1002/2014GL059345).
- Larkin, N. K., and D. E. Harrison, 2005: On the definition of El Niño and associated seasonal average U.S. weather anomalies. *Geophys. Res. Lett.*, **32**, L13705, doi:[10.1029/2005GL022738](https://doi.org/10.1029/2005GL022738).
- Latif, M., and T. P. Barnett, 1994: Causes of decadal climate variability over the North Pacific and North America. *Science*, **266**, 634–637, doi:[10.1126/science.266.5185.634](https://doi.org/10.1126/science.266.5185.634).
- , and —, 1996: Decadal climate variability over the North Pacific and North America: Dynamics and predictability. *J. Climate*, **9**, 2407–2423, doi:[10.1175/1520-0442\(1996\)009<2407:DCVOTN>2.0.CO;2](https://doi.org/10.1175/1520-0442(1996)009<2407:DCVOTN>2.0.CO;2).
- Lau, N.-C., 1997: Interactions between global SST anomalies and the midlatitude atmospheric circulation. *Bull. Amer. Meteor. Soc.*, **78**, 21–33, doi:[10.1175/1520-0477\(1997\)078<0021:IBGSA>2.0.CO;2](https://doi.org/10.1175/1520-0477(1997)078<0021:IBGSA>2.0.CO;2).
- , and M. J. Nath, 1994: A modeling study of the relative roles of tropical and extratropical SST anomalies in the variability of the global atmosphere–ocean system. *J. Climate*, **7**, 1184–1207, doi:[10.1175/1520-0442\(1994\)007<1184:AMSOTR>2.0.CO;2](https://doi.org/10.1175/1520-0442(1994)007<1184:AMSOTR>2.0.CO;2).
- , and —, 1996: The role of the “atmospheric bridge” in linking tropical Pacific ENSO events to extratropical SST anomalies. *J. Climate*, **9**, 2036–2057, doi:[10.1175/1520-0442\(1996\)009<2036:TROTBI>2.0.CO;2](https://doi.org/10.1175/1520-0442(1996)009<2036:TROTBI>2.0.CO;2).
- , and —, 2001: Impact of ENSO on SST variability in the North Pacific and North Atlantic: Seasonal dependence and role of extratropical air–sea coupling. *J. Climate*, **14**, 2846–2866, doi:[10.1175/1520-0442\(2001\)014<2846:IOEOSV>2.0.CO;2](https://doi.org/10.1175/1520-0442(2001)014<2846:IOEOSV>2.0.CO;2).
- Li, L., W. Li, and Y. Kushnir, 2012: Variation of the North Atlantic subtropical high western ridge and its implication to southeastern US summer precipitation. *Climate Dyn.*, **39**, 1401–1412, doi:[10.1007/s00382-011-1214-y](https://doi.org/10.1007/s00382-011-1214-y).
- Li, Y., F. Wang, and Y. Sun, 2012: Low-frequency spiciness variations in the tropical Pacific Ocean observed during 2003–2012. *Geophys. Res. Lett.*, **39**, L23601, doi:[10.1029/2012GL053971](https://doi.org/10.1029/2012GL053971).
- Lienert, F., J. C. Fyfe, and W. J. Merryfield, 2011: Do climate models capture the tropical influences on North Pacific sea surface temperature variability? *J. Climate*, **24**, 6203–6209, doi:[10.1175/JCLI-D-11-00205.1](https://doi.org/10.1175/JCLI-D-11-00205.1).
- Liu, Z., and M. A. Alexander, 2007: Atmospheric bridge, oceanic tunnel and global climatic teleconnections. *Rev. Geophys.*, **45**, RG2005, doi:[10.1029/2005RG000172](https://doi.org/10.1029/2005RG000172).

- MacDonald, G. M., and R. A. Case, 2005: Variations in the Pacific decadal oscillation over the past millennium. *Geophys. Res. Lett.*, **32**, L08703, doi:10.1029/2005GL022478.
- Mantua, N. J., S. R. Hare, Y. Zhang, J. M. Wallace, and R. C. Francis, 1997: A Pacific interdecadal climate oscillation with impacts on salmon production. *Bull. Amer. Meteor. Soc.*, **78**, 1069–1079, doi:10.1175/1520-0477(1997)078<1069:APICOW>2.0.CO;2.
- McCabe, G. J., and M. D. Dettinger, 1999: Decadal variations in the strength of ENSO teleconnections with precipitation in the western United States. *Int. J. Climatol.*, **19**, 1399–1410, doi:10.1002/(SICI)1097-0088(19991115)19:13<1399:AID-JOC457>3.0.CO;2-A.
- , and —, 2002: Primary modes and predictability of year-to-year snowpack variations in the western United States from teleconnections with Pacific Ocean climate. *J. Hydrometeor.*, **3**, 13–25, doi:10.1175/1525-7541(2002)003<0013:PMAPOY>2.0.CO;2.
- , M. A. Palecki, and J. L. Betancourt, 2004: Pacific and Atlantic Ocean influences on multidecadal drought frequency in the United States. *Proc. Natl. Acad. Sci. USA*, **101**, 4136–4141, doi:10.1073/pnas.0306738101.
- , T. R. Ault, B. I. Cook, J. L. Betancourt, and M. D. Schwartz, 2012: Influences of the El Niño Southern Oscillation and the Pacific decadal oscillation on the timing of the North American spring. *Int. J. Climatol.*, **32**, 2301–2310, doi:10.1002/joc.3400.
- McPhaden, M. J., and D. Zhang, 2002: Slowdown of the meridional overturning circulation in the upper Pacific Ocean. *Nature*, **415**, 603–608, doi:10.1038/415603a.
- Meehl, G. A., and H. Teng, 2014: CMIP5 multi-model hindcasts for the mid-1970s shift and early 2000s hiatus and predictions for 2016–2035. *Geophys. Res. Lett.*, **41**, 1711–1716, doi:10.1002/2014GL059256.
- , A. Hu, and B. D. Santer, 2009: The mid-1970s climate shift in the Pacific and the relative roles of forced versus inherent decadal variability. *J. Climate*, **22**, 780–792, doi:10.1175/2008JCLI2552.1.
- Mehta, V. M., N. J. Rosenberg, and K. Mendoza, 2012: Simulated impacts of three decadal climate variability phenomena on dryland corn and wheat yields in the Missouri River basin. *Agric. For. Meteor.*, **152**, 109–124, doi:10.1016/j.agrmet.2011.09.011.
- Mestas-Nuñez, A. M., and D. B. Enfield, 1999: Rotated global modes of non-ENSO sea surface temperature variability. *J. Climate*, **12**, 2734–2746, doi:10.1175/1520-0442(1999)012<2734:RGMONE>2.0.CO;2.
- Miller, A. J., and N. Schneider, 2000: Interdecadal climate regime dynamics in the North Pacific Ocean: Theories, observations and ecosystem impacts. *Prog. Oceanogr.*, **47**, 355–379, doi:10.1016/S0079-6611(00)00044-6.
- , D. R. Cayan, T. P. Barnett, N. E. Graham, and J. M. Oberhuber, 1994a: Interdecadal variability of the Pacific Ocean: Model response to observed heat flux and wind stress anomalies. *Climate Dyn.*, **9**, 287–302, doi:10.1007/BF00204744.
- , —, —, —, and —, 1994b: The 1976–77 climate shift of the Pacific Ocean. *Oceanography*, **7**, 21–26, doi:10.5670/oceanog.1994.11.
- , —, and W. B. White, 1998: A westward-intensified decadal change in the North Pacific thermocline and gyre-scale circulation. *J. Climate*, **11**, 3112–3127, doi:10.1175/1520-0442(1998)011<3112:AWIDCI>2.0.CO;2.
- Milotti, E., 1995: Linear processes that produce 1/f or flicker noise. *Phys. Rev. E*, **51**, 3087–3103, doi:10.1103/PhysRevE.51.3087.
- Minobe, S., 1997: A 50–70 year climatic oscillation over the North Pacific and North America. *Geophys. Res. Lett.*, **24**, 683–686, doi:10.1029/97GL00504.
- , 1999: Resonance in bidecadal and pentadecadal climate oscillations over the North Pacific: Role in climatic regime shifts. *Geophys. Res. Lett.*, **26**, 855–858, doi:10.1029/1999GL900119.
- Miyasaka, T., and H. Nakamura, 2005: Summertime subtropical highs and tropospheric planetary waves in the Northern Hemisphere. *J. Climate*, **18**, 5046–5065, doi:10.1175/JCLI3599.1.
- , —, B. Taguchi, and M. Nonaka, 2014: Multidecadal modulations of the low-frequency climate variability in the wintertime North Pacific since 1950. *Geophys. Res. Lett.*, **41**, 2948–2955, doi:10.1002/2014GL059696.
- Mo, K. C., 2010: Interdecadal modulation of the impact of ENSO on precipitation and temperature over the United States. *J. Climate*, **23**, 3639–3656, doi:10.1175/2010JCLI3553.1.
- Nakamura, H., and T. Yamagata, 1999: Recent decadal SST variability in the northwestern Pacific and associated atmospheric anomalies. *Beyond El Niño: Decadal and Interdecadal Climate Variability*, A. Navarra, Ed., Springer, 49–72.
- , and A. S. Kazmin, 2003: Decadal changes in the North Pacific oceanic frontal zones as revealed in ship and satellite observations. *J. Geophys. Res.*, **108**, 3078, doi:10.1029/1999JC000085.
- , G. Lin, and T. Yamagata, 1997: Decadal climate variability in the North Pacific during the recent decades. *Bull. Amer. Meteor. Soc.*, **78**, 2215–2225, doi:10.1175/1520-0477(1997)078<2215:DCVITN>2.0.CO;2.
- , T. Sampe, Y. Tanimoto, and A. Shimpo, 2004: Observed associations among storm tracks, jet streams and midlatitude oceanic fronts. *Earth's Climate: The Ocean–Atmosphere Interaction*, *Geophys. Monogr.*, Vol. 147, Amer. Geophys. Union, 329–346.
- Namias, J., and R. M. Born, 1970: Temporal coherence in North Pacific sea-surface temperature patterns. *J. Geophys. Res.*, **75**, 5952–5955, doi:10.1029/JC075i030p05952.
- , and —, 1974: Further studies of temporal coherence in North Pacific sea surface temperatures. *J. Geophys. Res.*, **79**, 797–798, doi:10.1029/JC079i006p00797.
- Newman, M., 2007: Interannual to decadal predictability of tropical and North Pacific sea surface temperatures. *J. Climate*, **20**, 2333–2356, doi:10.1175/JCLI4165.1.
- , 2013: An empirical benchmark for decadal forecasts of global surface temperature anomalies. *J. Climate*, **26**, 5260–5269, doi:10.1175/JCLI-D-12-00590.1.
- , G. P. Compo, and M. Alexander, 2003: ENSO-forced variability of the Pacific decadal oscillation. *J. Climate*, **16**, 3853–3857, doi:10.1175/1520-0442(2003)016<3853:EVOTPD>2.0.CO;2.
- , P. D. Sardeshmukh, and C. Penland, 2009: How important is air-sea coupling in ENSO and MJO evolution? *J. Climate*, **22**, 2958–2977, doi:10.1175/2008JCLI2659.1.
- , S.-I. Shin, and M. A. Alexander, 2011: Natural variation in ENSO flavors. *Geophys. Res. Lett.*, **38**, L14705, doi:10.1029/2011GL047658.
- Nonaka, M., H. Nakamura, Y. Tanimoto, T. Kagimoto, and H. Sasaki, 2006: Decadal variability in the Kuroshio–Oyashio Extension simulated in an eddy-resolving OGCM. *J. Climate*, **19**, 1970–1989, doi:10.1175/JCLI3793.1.
- , —, —, —, and —, 2008: Interannual-to-decadal variability in the Oyashio and its influence on temperature in the subarctic frontal zone: An eddy-resolving OGCM simulation. *J. Climate*, **21**, 6283–6303, doi:10.1175/2008JCLI2294.1.

- , H. Sasaki, B. Taguchi, and H. Nakamura, 2012: Potential predictability of interannual variability in the Kuroshio Extension jet speed in an eddy-resolving OGCM. *J. Climate*, **25**, 3645–3652, doi:[10.1175/JCLI-D-11-00641.1](https://doi.org/10.1175/JCLI-D-11-00641.1).
- , Y. Sasaki, H. Sasaki, B. Taguchi, and H. Nakamura, 2016: How potentially predictable are midlatitude ocean currents? *Sci. Rep.*, **6**, 20153, doi:[10.1038/srep20153](https://doi.org/10.1038/srep20153).
- Norris, J. R., 1998: Low cloud type over the ocean from surface observations. Part II: Geographic and seasonal variations. *J. Climate*, **11**, 383–403, doi:[10.1175/1520-0442\(1998\)011<0383:LCTOTO>2.0.CO;2](https://doi.org/10.1175/1520-0442(1998)011<0383:LCTOTO>2.0.CO;2).
- , Y. Zhang, and J. M. Wallace, 1998: Role of clouds in summertime atmosphere–ocean interactions over the North Pacific. *J. Climate*, **11**, 2482–2490, doi:[10.1175/1520-0442\(1998\)011<2482:ROLCLIS>2.0.CO;2](https://doi.org/10.1175/1520-0442(1998)011<2482:ROLCLIS>2.0.CO;2).
- Oakley, N. S., and K. T. Redmond, 2014: A climatology of 500-hPa closed lows in the northeastern Pacific Ocean, 1948–2011. *J. Appl. Meteor. Climatol.*, **53**, 1578–1592, doi:[10.1175/JAMC-D-13-0223.1](https://doi.org/10.1175/JAMC-D-13-0223.1).
- Okajima, S., H. Nakamura, K. Nishii, T. Miyasaka, and A. Kuwano-Yoshida, 2014: Assessing the importance of prominent warm SST anomalies over the midlatitude North Pacific in forcing large-scale atmospheric anomalies during 2011 summer and autumn. *J. Climate*, **27**, 3889–3903, doi:[10.1175/JCLI-D-13-00140.1](https://doi.org/10.1175/JCLI-D-13-00140.1).
- O'Reilly, C. H., and A. Czaja, 2015: The response of the Pacific storm track and atmospheric circulation to Kuroshio Extension variability. *Quart. J. Roy. Meteor. Soc.*, **141**, 52–66, doi:[10.1002/qj.2334](https://doi.org/10.1002/qj.2334).
- Oshima, K., and Y. Tanimoto, 2009: An evaluation of reproducibility of the Pacific decadal oscillation in the CMIP3 simulations. *J. Meteor. Soc. Japan*, **87**, 755–770, doi:[10.2151/jmsj.87.755](https://doi.org/10.2151/jmsj.87.755).
- Overland, J. E., D. B. Percival, and H. O. Mofjeld, 2006: Regime shifts and red noise in the North Pacific. *Deep-Sea Res. I*, **53**, 582–588, doi:[10.1016/j.dsr.2005.12.011](https://doi.org/10.1016/j.dsr.2005.12.011).
- Park, J.-H., S. I. An, S.-W. Yeh, and N. Schneider, 2013: Quantitative assessment of the climate components driving the Pacific decadal oscillation in climate models. *Theor. Appl. Climatol.*, **112**, 431–445, doi:[10.1007/s00704-012-0730-y](https://doi.org/10.1007/s00704-012-0730-y).
- Parker, D., C. Folland, A. Scaife, J. Knight, A. Colman, P. Baines, and B. Dong, 2007: Decadal to multidecadal variability and the climate change background. *J. Geophys. Res.*, **112**, D18115, doi:[10.1029/2007JD008411](https://doi.org/10.1029/2007JD008411).
- Pederson, G. T., S. T. Gray, T. Ault, W. Marsh, D. B. Fagre, A. G. Bunn, C. A. Woodhouse, and L. J. Graumlich, 2011: Climatic controls on the snowmelt hydrology of the northern Rocky Mountains. *J. Climate*, **24**, 1666–1687, doi:[10.1175/2010JCLI3729.1](https://doi.org/10.1175/2010JCLI3729.1).
- Penland, C., and P. D. Sardeshmukh, 1995: The optimal growth of tropical sea surface temperature anomalies. *J. Climate*, **8**, 1999–2024, doi:[10.1175/1520-0442\(1995\)008<1999:TOGOTS>2.0.CO;2](https://doi.org/10.1175/1520-0442(1995)008<1999:TOGOTS>2.0.CO;2).
- , and —, 2012: Alternative interpretations of power-law distributions found in nature. *Chaos*, **22**, 023119, doi:[10.1063/1.4706504](https://doi.org/10.1063/1.4706504).
- Percival, D. B., J. E. Overland, and H. O. Mofjeld, 2001: Interpretation of North Pacific variability as a short- and long-memory process. *J. Climate*, **14**, 4545–4559, doi:[10.1175/1520-0442\(2001\)014<4545:IONPVA>2.0.CO;2](https://doi.org/10.1175/1520-0442(2001)014<4545:IONPVA>2.0.CO;2).
- Phillips, A. S., C. Deser, and J. Fasullo, 2014: A new tool for evaluating modes of variability in climate models. *Eos*, *Trans. Amer. Geophys. Union*, **95**, 453–455, doi:[10.1002/2014EO490002](https://doi.org/10.1002/2014EO490002).
- Pierce, D. W., 2001: Distinguishing coupled ocean–atmosphere interactions from background noise in the North Pacific. *Prog. Oceanogr.*, **49**, 331–352, doi:[10.1016/S0079-6611\(01\)00029-5](https://doi.org/10.1016/S0079-6611(01)00029-5).
- , 2002: The role of sea surface temperatures in interactions between ENSO and the North Pacific Oscillation. *J. Climate*, **15**, 1295–1308, doi:[10.1175/1520-0442\(2002\)015<1295:TROSST>2.0.CO;2](https://doi.org/10.1175/1520-0442(2002)015<1295:TROSST>2.0.CO;2).
- Polade, S. D., A. Gershunov, D. R. Cayan, M. D. Dettinger, and D. W. Pierce, 2013: Natural climate variability and teleconnections to precipitation over the Pacific–North American region in CMIP3 and CMIP5 models. *Geophys. Res. Lett.*, **40**, 2296–2301, doi:[10.1002/grl.50491](https://doi.org/10.1002/grl.50491).
- Power, S., T. Casey, C. Folland, A. Colman, and V. Mehta, 1999: Inter-decadal modulation of the impact of ENSO on Australia. *Climate Dyn.*, **15**, 319–324, doi:[10.1007/s003820050284](https://doi.org/10.1007/s003820050284).
- Qiu, B., 2000: Interannual variability of the Kuroshio Extension system and its impact on the wintertime SST field. *J. Phys. Oceanogr.*, **30**, 1486–1502, doi:[10.1175/1520-0485\(2000\)030<1486:IVOTKE>2.0.CO;2](https://doi.org/10.1175/1520-0485(2000)030<1486:IVOTKE>2.0.CO;2).
- , 2002: The Kuroshio Extension system: Its large-scale variability and role in the midlatitude ocean–atmosphere interaction. *J. Oceanogr.*, **58**, 57–75, doi:[10.1023/A:1015824717293](https://doi.org/10.1023/A:1015824717293).
- , 2003: Kuroshio Extension variability and forcing of the Pacific decadal oscillations: Responses and potential feedback. *J. Phys. Oceanogr.*, **33**, 2465–2482, doi:[10.1175/2459.1](https://doi.org/10.1175/2459.1).
- , and S. Chen, 2005: Variability of the Kuroshio Extension jet, recirculation gyre, and mesoscale eddies on decadal time scales. *J. Phys. Oceanogr.*, **35**, 2090–2103, doi:[10.1175/JPO2807.1](https://doi.org/10.1175/JPO2807.1).
- , and —, 2010: Eddy-mean flow interaction in the decadally modulating Kuroshio Extension system. *Deep-Sea Res. II*, **57**, 1098–1110, doi:[10.1016/j.dsr2.2008.11.036](https://doi.org/10.1016/j.dsr2.2008.11.036).
- , N. Schneider, and S. Chen, 2007: Coupled decadal variability in the North Pacific: An observationally constrained idealized model. *J. Climate*, **20**, 3602–3620, doi:[10.1175/JCLI4190.1](https://doi.org/10.1175/JCLI4190.1).
- , S. Chen, N. Schneider, and B. Taguchi, 2014: A coupled decadal prediction of the dynamic state of the Kuroshio Extension system. *J. Climate*, **27**, 1751–1764, doi:[10.1175/JCLI-D-13-00318.1](https://doi.org/10.1175/JCLI-D-13-00318.1).
- Rayner, N. A., D. E. Parker, E. B. Horton, C. K. Folland, L. V. Alexander, D. P. Rowell, E. C. Kent, and A. Kaplan, 2003: Global analyses of sea surface temperature, sea ice, and night marine air temperature since the late nineteenth century. *J. Geophys. Res.*, **108**, 4407, doi:[10.1029/2002JD002670](https://doi.org/10.1029/2002JD002670).
- Reynolds, R. W., T. M. Smith, C. Liu, D. B. Chelton, K. S. Casey, and M. G. Schlax, 2007: Daily high-resolution blended analyses for sea surface temperature. *J. Climate*, **20**, 5473–5496, doi:[10.1175/2007JCLI1824.1](https://doi.org/10.1175/2007JCLI1824.1).
- Rodgers, K. B., P. Friederichs, and M. Latif, 2004: Tropical Pacific decadal variability and its relation to decadal modulation of ENSO. *J. Climate*, **17**, 3761–3774, doi:[10.1175/1520-0442\(2004\)017<3761:TPDVAI>2.0.CO;2](https://doi.org/10.1175/1520-0442(2004)017<3761:TPDVAI>2.0.CO;2).
- Rudnick, D. L., and R. E. Davis, 2003: Red noise and regime shifts. *Deep-Sea Res. I*, **50**, 691–699, doi:[10.1016/S0967-0637\(03\)00053-0](https://doi.org/10.1016/S0967-0637(03)00053-0).
- Saravanan, R., and J. C. McWilliams, 1998: Advective ocean–atmosphere interaction: An analytical stochastic model with implications for decadal variability. *J. Climate*, **11**, 165–188, doi:[10.1175/1520-0442\(1998\)011<0165:AOAIAA>2.0.CO;2](https://doi.org/10.1175/1520-0442(1998)011<0165:AOAIAA>2.0.CO;2).

- Sardeshmukh, P. D., G. P. Compo, and C. Penland, 2000: Changes of probability associated with El Niño. *J. Climate*, **13**, 4268–4286, doi:[10.1175/1520-0442\(2000\)013<4268:COPAWE>2.0.CO;2](https://doi.org/10.1175/1520-0442(2000)013<4268:COPAWE>2.0.CO;2).
- Sasaki, Y. N., and N. Schneider, 2011: Decadal shifts of the Kuroshio Extension jet: Application of thin-jet theory. *J. Phys. Oceanogr.*, **41**, 979–993, doi:[10.1175/2010JPO4550.1](https://doi.org/10.1175/2010JPO4550.1).
- , —, N. Maximenko, and K. Lebedev, 2010: Observational evidence for propagation of decadal spiciness anomalies in the North Pacific. *Geophys. Res. Lett.*, **37**, L07708, doi:[10.1029/2010GL042716](https://doi.org/10.1029/2010GL042716).
- , S. Minobe, and N. Schneider, 2013: Decadal response of the Kuroshio Extension jet to Rossby waves: Observation and thin-jet theory. *J. Phys. Oceanogr.*, **43**, 442–456, doi:[10.1175/JPO-D-12-096.1](https://doi.org/10.1175/JPO-D-12-096.1).
- Schneider, N., and A. J. Miller, 2001: Predicting western North Pacific Ocean climate. *J. Climate*, **14**, 3997–4002, doi:[10.1175/1520-0442\(2001\)014<3997:PWNPOC>2.0.CO;2](https://doi.org/10.1175/1520-0442(2001)014<3997:PWNPOC>2.0.CO;2).
- , and B. D. Cornuelle, 2005: The forcing of the Pacific decadal oscillation. *J. Climate*, **18**, 4355–4373, doi:[10.1175/JCLI3527.1](https://doi.org/10.1175/JCLI3527.1).
- , A. J. Miller, M. A. Alexander, and C. Deser, 1999: Subduction of decadal North Pacific temperature anomalies: Observations and dynamics. *J. Phys. Oceanogr.*, **29**, 1056–1070, doi:[10.1175/1520-0485\(1999\)029<1056:SODNPT>2.0.CO;2](https://doi.org/10.1175/1520-0485(1999)029<1056:SODNPT>2.0.CO;2).
- , —, and D. W. Pierce, 2002: Anatomy of North Pacific decadal variability. *J. Climate*, **15**, 586–605, doi:[10.1175/1520-0442\(2002\)015<0586:AONPDV>2.0.CO;2](https://doi.org/10.1175/1520-0442(2002)015<0586:AONPDV>2.0.CO;2).
- Schwartz, R. E., A. Gershunov, S. F. Iacobellis, and D. R. Cayan, 2014: North American west coast summer low cloudiness: Broad scale variability associated with sea surface temperature. *Geophys. Res. Lett.*, **41**, 3307–3314, doi:[10.1002/2014GL059825](https://doi.org/10.1002/2014GL059825).
- Seager, R., Y. Kushnir, N. H. Naik, M. A. Cane, and J. Miller, 2001: Wind-driven shifts in the latitude of the Kuroshio–Oyashio extension and generation of SST anomalies on decadal timescales. *J. Climate*, **14**, 4249–4265, doi:[10.1175/1520-0442\(2001\)014<4249:WDSITL>2.0.CO;2](https://doi.org/10.1175/1520-0442(2001)014<4249:WDSITL>2.0.CO;2).
- , A. R. Karspeck, M. A. Cane, Y. Kushnir, A. Giannini, A. Kaplan, B. Kerman, and J. Velez, 2004: Predicting Pacific decadal variability. *Earth's Climate: The Ocean–Atmosphere Interaction, Geophys. Monogr.*, Vol. 147, Amer. Geophys. Union, 105–120.
- Shakun, J. D., and J. Shaman, 2009: Tropical origins of North and South Pacific decadal variability. *Geophys. Res. Lett.*, **36**, L19711, doi:[10.1029/2009GL040313](https://doi.org/10.1029/2009GL040313).
- Sheffield, J., and Coauthors, 2013: North American climate in CMIP5 experiments. Part II: Evaluation of historical simulations of intraseasonal to decadal variability. *J. Climate*, **26**, 9247–9290, doi:[10.1175/JCLI-D-12-00593.1](https://doi.org/10.1175/JCLI-D-12-00593.1).
- Shen, C., W.-C. Wang, W. Gong, and Z. Hao, 2006: A Pacific decadal oscillation record since 1470 AD reconstructed from proxy data of summer rainfall over eastern China. *Geophys. Res. Lett.*, **33**, L03702, doi:[10.1029/2005GL024804](https://doi.org/10.1029/2005GL024804).
- Smirnov, D., M. Newman, and M. A. Alexander, 2014: Investigating the role of ocean–atmosphere coupling in the North Pacific Ocean. *J. Climate*, **27**, 592–606, doi:[10.1175/JCLI-D-13-00123.1](https://doi.org/10.1175/JCLI-D-13-00123.1).
- , —, —, Y.-O. Kwon, and C. Frankignoul, 2015: Investigating the local atmospheric response to a realistic shift in the Oyashio sea surface temperature front. *J. Climate*, **28**, 1126–1147, doi:[10.1175/JCLI-D-14-00285.1](https://doi.org/10.1175/JCLI-D-14-00285.1).
- Smith, T. M., R. W. Reynolds, T. C. Peterson, and J. Lawrimore, 2008: Improvements to NOAA's historical merged land–ocean temperature analysis (1880–2006). *J. Climate*, **21**, 2283–2296, doi:[10.1175/2007JCLI2100.1](https://doi.org/10.1175/2007JCLI2100.1).
- Stewart, I. T., D. R. Cayan, and M. D. Dettinger, 2005: Changes toward earlier streamflow timing across western North America. *J. Climate*, **18**, 1136–1155, doi:[10.1175/JCLI3321.1](https://doi.org/10.1175/JCLI3321.1).
- St. George, S., 2014: An overview of tree-ring width records across the Northern Hemisphere. *Quat. Sci. Rev.*, **95**, 132–150, doi:[10.1016/j.quascirev.2014.04.029](https://doi.org/10.1016/j.quascirev.2014.04.029).
- Strong, C., and G. Magnusdottir, 2009: The role of tropospheric Rossby wave breaking in the Pacific decadal oscillation. *J. Climate*, **22**, 1819–1833, doi:[10.1175/2008JCLI2593.1](https://doi.org/10.1175/2008JCLI2593.1).
- Sugimoto, S., and K. Hanawa, 2011: Roles of SST anomalies on the wintertime turbulent heat fluxes in the Kuroshio–Oyashio confluence region: Influences of warm eddies detached from the Kuroshio Extension. *J. Climate*, **24**, 6551–6561, doi:[10.1175/2011JCLI4023.1](https://doi.org/10.1175/2011JCLI4023.1).
- Taguchi, B., S.-P. Xie, N. Schneider, M. Nonaka, H. Sasaki, and Y. Sasai, 2007: Decadal variability of the Kuroshio Extension: Observations and an eddy-resolving model hindcast. *J. Climate*, **20**, 2357–2377, doi:[10.1175/JCLI4142.1](https://doi.org/10.1175/JCLI4142.1).
- , H. Nakamura, M. Nonaka, N. Komori, A. Kuwano-Yoshida, K. Takaya, and A. Goto, 2012: Seasonal evolutions of atmospheric response to decadal SST anomalies in the North Pacific subarctic frontal zone: Observations and a coupled model simulation. *J. Climate*, **25**, 111–139, doi:[10.1175/JCLI-D-11-00046.1](https://doi.org/10.1175/JCLI-D-11-00046.1).
- Takahashi, K., A. Montecinos, K. Goubanova, and B. Dewitte, 2011: ENSO regimes: Reinterpreting the canonical and Modoki El Niño. *Geophys. Res. Lett.*, **38**, L10704, doi:[10.1029/2011GL047364](https://doi.org/10.1029/2011GL047364).
- Tanimoto, Y., H. Nakamura, T. Kagimoto, and S. Yamane, 2003: An active role of extratropical sea surface temperature anomalies in determining anomalous turbulent heat fluxes. *J. Geophys. Res.*, **108**, 3304, doi:[10.1029/2002JC001750](https://doi.org/10.1029/2002JC001750).
- Taylor, K. E., 2001: Summarizing multiple aspects of model performance in a single diagram. *J. Geophys. Res.*, **106**, 7183–7192, doi:[10.1029/2000JD900719](https://doi.org/10.1029/2000JD900719).
- Timlin, M. S., M. A. Alexander, and C. Deser, 2002: On the reemergence of North Atlantic SST anomalies. *J. Climate*, **15**, 2707–2712, doi:[10.1175/1520-0442\(2002\)015<2707:OTRONA>2.0.CO;2](https://doi.org/10.1175/1520-0442(2002)015<2707:OTRONA>2.0.CO;2).
- Tingley, M. P., P. F. Craigmile, M. Haran, B. Li, E. Mannhardt, and B. Rajaratnam, 2012: Piecing together the past: Statistical insights into paleoclimatic reconstructions. *Quat. Sci. Rev.*, **35**, 1–22, doi:[10.1016/j.quascirev.2012.01.012](https://doi.org/10.1016/j.quascirev.2012.01.012).
- Trenberth, K. E., and J. W. Hurrell, 1994: Decadal atmosphere–ocean variations in the Pacific. *Climate Dyn.*, **9**, 303–319, doi:[10.1007/BF00204745](https://doi.org/10.1007/BF00204745).
- , and D. P. Stepaniak, 2001: Indices of El Niño evolution. *J. Climate*, **14**, 1697–1701, doi:[10.1175/1520-0442\(2001\)014<1697:LIOENO>2.0.CO;2](https://doi.org/10.1175/1520-0442(2001)014<1697:LIOENO>2.0.CO;2).
- , G. W. Branstator, D. Karoly, A. Kumar, N.-C. Lau, and C. Ropelewski, 1998: Progress during TOGA in understanding and modeling global teleconnections associated with tropical sea surface temperatures. *J. Geophys. Res.*, **103**, 14 291–14 324, doi:[10.1029/97JC01444](https://doi.org/10.1029/97JC01444).
- Van Oldenborgh, G. J., F. J. Doblas-Reyes, B. Wouters, and W. Hazleger, 2012: Skill in the trend and internal variability in a multi-model decadal prediction ensemble. *Climate Dyn.*, **38**, 1263–1280, doi:[10.1007/s00382-012-1313-4](https://doi.org/10.1007/s00382-012-1313-4).
- Vimont, D. J., 2005: The contribution of the interannual ENSO cycle to the spatial pattern of decadal ENSO-like variability. *J. Climate*, **18**, 2080–2092, doi:[10.1175/JCLI3365.1](https://doi.org/10.1175/JCLI3365.1).

- , D. S. Battisti, and A. C. Hirst, 2001: Footprinting: A seasonal link between the mid-latitudes and tropics. *Geophys. Res. Lett.*, **28**, 3923–3926, doi:[10.1029/2001GL013435](https://doi.org/10.1029/2001GL013435).
- , J. M. Wallace, and D. S. Battisti, 2003: The seasonal footprinting mechanism in the Pacific: Implications for ENSO. *J. Climate*, **16**, 2668–2675, doi:[10.1175/1520-0442\(2003\)016<2668:TSFMIT>2.0.CO;2](https://doi.org/10.1175/1520-0442(2003)016<2668:TSFMIT>2.0.CO;2).
- , M. Alexander, and A. Fontaine, 2009: Midlatitude excitation of tropical variability in the Pacific: The role of thermodynamic coupling and seasonality. *J. Climate*, **22**, 518–534, doi:[10.1175/2008JCLI2220.1](https://doi.org/10.1175/2008JCLI2220.1).
- Vose, R. S., and Coauthors, 2014: Improved historical temperature and precipitation time series for U.S. climate divisions. *J. Appl. Meteor. Climatol.*, **53**, 1232–1251, doi:[10.1175/JAMC-D-13-0248.1](https://doi.org/10.1175/JAMC-D-13-0248.1).
- Walker, G. T., and E. W. Bliss, 1932: World weather V. *Mem. Royal Meteor. Soc.*, **4** (36), 53–84.
- Wang, H., A. Kumar, W. Wang, and Y. Xue, 2012: Seasonality of the Pacific decadal oscillation. *J. Climate*, **25**, 25–38, doi:[10.1175/2011JCLI4092.1](https://doi.org/10.1175/2011JCLI4092.1).
- Wang, S., J. Huang, Y. He, and Y. Guan, 2014: Combined effects of the Pacific decadal oscillation and El Niño–Southern Oscillation on global land dry–wet changes. *Sci. Rep.*, **4**, 6651, doi:[10.1038/srep06651](https://doi.org/10.1038/srep06651).
- Wang, S.-Y., M. L’Heureux, and H.-H. Chia, 2012: ENSO prediction one year in advance using western North Pacific sea surface temperatures. *Geophys. Res. Lett.*, **39**, L05702, doi:[10.1029/2012GL050909](https://doi.org/10.1029/2012GL050909).
- Wen, C., Y. Xue, and A. Kumar, 2012: Seasonal prediction of North Pacific SSTs and PDO in the NCEP CFS hindcasts. *J. Climate*, **25**, 5689–5710, doi:[10.1175/JCLI-D-11-00556.1](https://doi.org/10.1175/JCLI-D-11-00556.1).
- , A. Kumar, and Y. Xue, 2014: Factors contributing to uncertainty in Pacific decadal oscillation index. *Geophys. Res. Lett.*, **41**, 7980–7986, doi:[10.1002/2014GL061992](https://doi.org/10.1002/2014GL061992).
- Wittenberg, A. T., A. Rosati, T. L. Delworth, G. A. Vecchi, and F. Zeng, 2014: ENSO modulation: Is it decadally predictable? *J. Climate*, **27**, 2667–2681, doi:[10.1175/JCLI-D-13-00577.1](https://doi.org/10.1175/JCLI-D-13-00577.1).
- Wood, R., 2012: Stratocumulus clouds. *Mon. Wea. Rev.*, **140**, 2373–2423, doi:[10.1175/MWR-D-11-00121.1](https://doi.org/10.1175/MWR-D-11-00121.1).
- Wu, A., W. W. Hsieh, and A. Shabbar, 2005: The nonlinear patterns of North American winter temperature and precipitation associated with ENSO. *J. Climate*, **18**, 1736–1752, doi:[10.1175/JCLI3372.1](https://doi.org/10.1175/JCLI3372.1).
- Wu, L., Z. Liu, R. Gallimore, R. Jacob, D. Lee, and Y. Zhong, 2003: Pacific decadal variability: The tropical Pacific mode and the North Pacific mode. *J. Climate*, **16**, 1101–1120, doi:[10.1175/1520-0442\(2003\)16<1101:PDVTTP>2.0.CO;2](https://doi.org/10.1175/1520-0442(2003)16<1101:PDVTTP>2.0.CO;2).
- Yeh, S.-W., and B. P. Kirtman, 2008: The low-frequency relationship of the tropical–North Pacific sea surface temperature teleconnections. *J. Climate*, **21**, 3416–3432, doi:[10.1175/2007JCLI1648.1](https://doi.org/10.1175/2007JCLI1648.1).
- , X. Wang, C. Wang, and B. Dewitte, 2015: On the relationship between the North Pacific climate variability and the central Pacific El Niño. *J. Climate*, **28**, 663–677, doi:[10.1175/JCLI-D-14-00137.1](https://doi.org/10.1175/JCLI-D-14-00137.1).
- Yim, B. Y., M. Kwon, H. S. Min, and J.-S. Kug, 2014: Pacific decadal oscillation and its relation to the extratropical atmospheric variation in CMIP5. *Climate Dyn.*, **44**, 1521–1540, doi:[10.1007/s00382-014-2349-4](https://doi.org/10.1007/s00382-014-2349-4).
- Yu, B., and F. W. Zwiers, 2007: The impact of combined ENSO and PDO on the PNA climate: A 1,000-year climate modeling study. *Climate Dyn.*, **29**, 837–851, doi:[10.1007/s00382-007-0267-4](https://doi.org/10.1007/s00382-007-0267-4).
- Yu, J.-Y., Y. Zou, S. T. Kim, and T. Lee, 2012: The changing impact of El Niño on US winter temperatures. *Geophys. Res. Lett.*, **39**, L15702, doi:[10.1029/2012GL052483](https://doi.org/10.1029/2012GL052483).
- Zhang, D., and M. J. McPhaden, 2006: Decadal variability of the shallow Pacific meridional overturning circulation: Relation to tropical sea surface temperatures in observations and climate change models. *Ocean Modell.*, **15**, 250–273, doi:[10.1016/j.ocemod.2005.12.005](https://doi.org/10.1016/j.ocemod.2005.12.005).
- Zhang, L., and T. L. Delworth, 2015: Analysis of the characteristics and mechanisms of the Pacific decadal oscillation in a suite of coupled models from the Geophysical Fluid Dynamics Laboratory. *J. Climate*, **28**, 7678–7701, doi:[10.1175/JCLI-D-14-00647.1](https://doi.org/10.1175/JCLI-D-14-00647.1).
- Zhang, X., J. Wang, F. W. Zwiers, and P. Y. Groisman, 2010: The influence of large-scale climate variability on winter maximum daily precipitation over North America. *J. Climate*, **23**, 2902–2915, doi:[10.1175/2010JCLI3249.1](https://doi.org/10.1175/2010JCLI3249.1).
- Zhang, Y., J. M. Wallace, and D. S. Battisti, 1997: ENSO-like interdecadal variability: 1900–93. *J. Climate*, **10**, 1004–1020, doi:[10.1175/1520-0442\(1997\)010<1004:ELIV>2.0.CO;2](https://doi.org/10.1175/1520-0442(1997)010<1004:ELIV>2.0.CO;2).
- Zhong, Y., Z. Liu, and R. Jacob, 2008: Origin of Pacific multidecadal variability in Community Climate System Model, version 3 (CCSM3): A combined statistical and dynamical assessment. *J. Climate*, **21**, 114–133, doi:[10.1175/2007JCLI1730.1](https://doi.org/10.1175/2007JCLI1730.1).